CHAPTER

13

Geophysical Fluid Dynamics

OUTLINE

CHAPTER OBJECTIVES

- To introduce the approximations and phenomena that are common in geophysical fluid dynamics
- To describe flows near air-water interfaces and solid surfaces in steadily rotating coordinate systems

- To specify the effects of planetary rotation on waves in stratified fluids
- To describe the instabilities of very long waves that span a significant range of latitude
- To provide an introduction to geostrophic turbulence and the reversed energy cascade

13.1. INTRODUCTION

The subject of geophysical fluid dynamics deals with the dynamics of the atmosphere and the ocean. Motions within these fluid masses are intimately connected through continual exchanges of momentum, heat, and moisture, and cannot be considered separately on a global scale. The field has been largely developed by meteorologists and oceanographers, but nonspecialists have also been interested in the subject. Taylor was not a geophysical fluid dynamicist, but he held the position of a meteorologist for some time, and through this involvement he developed a special interest in the problems of turbulence and instability. Although Prandtl was mainly interested in the engineering aspects of fluid mechanics, his well-known textbook (Prandtl, 1952) contains several sections dealing with meteorological aspects of fluid mechanics. Notwithstanding the pressure for technical specialization, it is worthwhile to learn something of this fascinating field even if one's primary interest is in another area of fluid mechanics.

Together the atmosphere and ocean have a large and consequential impact on humanity. The combined dynamics of the atmosphere and ocean are leading contributors to global climate. We all live within the atmosphere and are almost helplessly affected by the weather and its rather chaotic behavior which modulates agricultural success. Ocean currents effect navigation, fisheries, and pollution disposal. Populations that occupy coastlines can do little to prevent hurricanes, typhoons, or tsunamis. Thus, understanding and reliably predicting geophysical fluid dynamic events and trends are scientific, economic, humanitarian, and even political priorities. This chapter provides the basic elements necessary for developing an understanding of geophysical fluid dynamics.

The two features that distinguish geophysical fluid dynamics from other areas of fluid dynamics are the rotation of the earth and the vertical density stratification of the medium. We shall see that these two effects dominate the dynamics to such an extent that entirely new classes of phenomena arise, which have no counterpart in the laboratory-scale flows emphasized in the preceding chapters. (For example, the dominant mode of flow in the atmosphere and the ocean is *along* the lines of constant pressure, not from high to low pressures.) The motion of the atmosphere and the ocean is naturally studied in a coordinate frame rotating with the earth. This gives rise to the Coriolis force (see Section 4.7). The density stratification gives rise to buoyancy forces (Section 4.11 and Chapter 7). In addition, important relevant material includes vorticity, boundary layers, instability, and turbulence (Chapters 5, 9, 11, and 12). The reader should be familiar with these topics before proceeding further with the present chapter.

Because Coriolis forces and stratification effects play dominating roles in both the atmosphere and the ocean, there is a great deal of similarity between the dynamics of these two media; this makes it possible to study them together. There are also significant differences, however. For example the effects of lateral boundaries, due to the presence of continents, are important in the ocean but less so in the atmosphere. The intense currents (like the Gulf Stream and the Kuroshio) along the western ocean boundaries have no atmospheric analog. On the other hand phenomena like cloud formation and latent heat release due to moisture condensation are typically atmospheric phenomena. Plus, processes are generally slower in the ocean, in which a typical horizontal velocity is 0.1 m/s, although velocities of the order of 1−2 m/s are found within the intense western boundary currents. In contrast, typical velocities in the atmosphere are 10−20 m/s. The nomenclature can also be different in the two fields. Meteorologists refer to a flow directed to the west as an "easterly wind" (i.e., *from* the east), while oceanographers refer to such a flow as a "westward current." Atmospheric scientists refer to vertical positions by *heights* measured upward from the earth's surface, while oceanographers refer to *depths* measured downward from the sea surface. However, we shall always take the vertical coordinate z to be upward, so no confusion should arise.

We shall see that rotational effects caused by the presence of the Coriolis force have opposite signs in the two hemispheres. Note that *all figures and descriptions given here are valid for the northern hemisphere.* In some cases the sense of the rotational effect for the southern hemisphere has been explicitly mentioned. When the sense of the rotational effect is left unspecified for the southern hemisphere, it has to be assumed as opposite to that in the northern hemisphere.

13.2. VERTICAL VARIATION OF DENSITY IN THE ATMOSPHERE AND OCEAN

An important variable in the study of geophysical fluid dynamics is the density stratification. In (1.35) we saw that the static stability of a fluid medium is determined by the sign of the potential density gradient:

$$\frac{d\rho_\theta}{dz} = \frac{d\rho}{dz} + \frac{g\rho}{c^2}, \tag{13.1}$$

where c is the speed of sound. A medium is statically stable if the potential density decreases with height. The first term on the right-hand side corresponds to the *in situ* density change due to all sources such as pressure, temperature, and concentration of a constituent such as the salinity in the sea or the water vapor in the atmosphere. The second term on the right side is the density gradient due to the pressure decrease with height in an adiabatic environment and is called the *adiabatic density gradient*. The corresponding temperature gradient is called the *adiabatic temperature gradient*. For incompressible fluids $c = \infty$ and the adiabatic density gradient is zero.

As shown in Section 1.10, the temperature of a dry adiabatic atmosphere decreases upward at the rate of $\approx 10^\circ$C/km; that of a moist atmosphere decreases at the rate of ≈ 5−6°C/km. In the ocean, the adiabatic density gradient is $g\rho/c^2 \sim 4 \times 10^{-3}$ kg/m^4,

for a typical sound speed of $c = 1520$ m/s. The potential density in the ocean increases with depth at a much smaller rate of 0.6×10^{-3} kg/m^4, so it follows that most of the *in situ* density increase with depth in the ocean is due to the compressibility effects and not to changes in temperature or salinity. As potential density is the variable that determines the static stability, oceanographers take into account the compressibility effects by referring all their density measurements to the sea-level pressure. Unless specified otherwise, throughout the present chapter potential density will simply be referred to as *density*, omitting the qualifier *potential*.

The mean vertical distribution of the *in situ* temperature in the lower 50 km of the atmosphere is shown in Figure 13.1. The lowest 10 km is called the *troposphere*, in which the temperature decreases with height at the rate of 6.5°C/km. This is close to the moist adiabatic lapse rate, which means that the troposphere is close to being neutrally stable. The neutral stability is expected because turbulent mixing due to frictional and convective effects in the lower atmosphere keeps it well stirred and therefore close to the neutral stratification. Practically all the clouds, weather changes, and water vapor of the atmosphere are found in the troposphere. The layer is capped by the *tropopause*, at an average height of 10 km, above which the temperature increases. This higher layer is called the *stratosphere*, because it is very stably stratified. The increase of temperature with height in this layer is caused by the absorption of the sun's ultraviolet rays by ozone. The stability of the layer inhibits mixing and

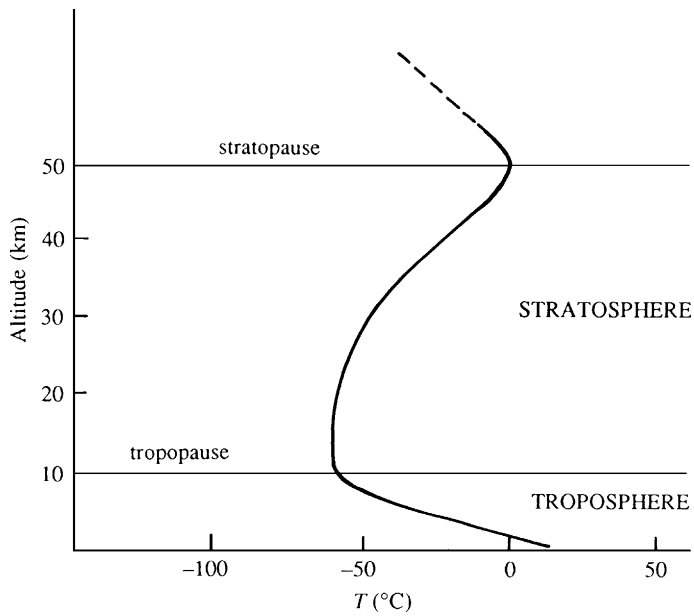

FIGURE 13.1 Sketch of the vertical distribution of temperature in the lower 50 km of the atmosphere. In the lowest layer, the troposphere, the temperature decreases with height and this is where nearly all weather occurs. The next layer is the stratosphere where temperature increases with height. The troposphere is separated from the stratosphere by the tropopause, and the stratosphere ends at the stratopause.

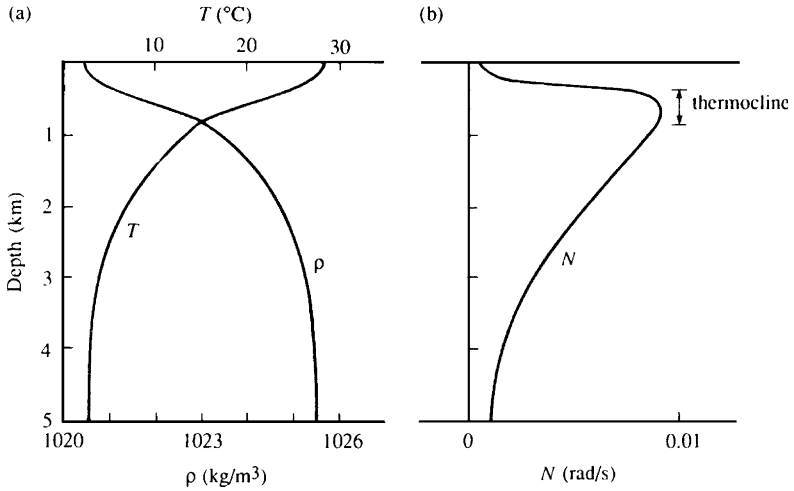

FIGURE 13.2 Typical vertical distributions of: (a) temperature and density, and (b) buoyancy frequency in the ocean. Temperature falls while density increases with increasing depth. The buoyancy frequency peaks in the region of the thermocline where temperature changes most rapidly with depth.

consequently acts as a lid on the turbulence and convective motion of the troposphere. The increase of temperature stops at the *stratopause* at a height of nearly 50 km.

The vertical structure of density in the ocean is sketched in Figure 13.2, showing typical profiles of potential density and temperature. Most of the temperature increase with height is due to the absorption of solar radiation within the upper layer of the ocean. The density distribution in the ocean is also affected by the salinity. However, there is no characteristic variation of salinity with depth, and a decrease with depth is found to be as common as an increase with depth. In most cases, however, the vertical structure of density in the ocean is determined mainly by that of temperature, the salinity effects being secondary. The upper 50−200 m of ocean is well mixed, due to the turbulence generated by the wind, waves, current shear, and the convective overturning caused by surface cooling. Temperature gradients decrease with depth, becoming quite small below a depth of 1500 m. There is usually a large temperature gradient in the depth range of 100−500 m. This layer of high stability is called the *thermocline*. Figure 13.2 also shows the profile of *buoyancy frequency* N, defined by

$$N^2 \equiv -\frac{g}{\rho_0}\frac{d\rho}{dz},$$

where ρ of course stands for the potential density and ρ_0 is a constant reference density (*cf*. (1.29) and (7.128)). The buoyancy frequency reaches a typical maximum value of $N_{\max} \sim 0.01\text{s}^{-1}$ (period $\sim$ 10 min) in the thermocline and decreases both upward and downward.

13.3. EQUATIONS OF MOTION

In this section we shall review the relevant equations of motion, which are derived and discussed in Chapter 4. The equations of motion for a stratified medium, observed in

a system of coordinates rotating at an angular velocity Ω with respect to the "fixed stars," are:

$$\nabla\cdot\mathbf{u} = 0, \quad \frac{D\mathbf{u}}{Dt} + 2\boldsymbol{\Omega}\times\mathbf{u} = \frac{1}{\rho_0}\nabla p - \frac{g\rho}{\rho_0}\mathbf{e}_z + \mathrm{F}, \text{ and } \frac{D\rho}{Dt} = 0, \tag{13.2}$$

where **F** is the friction force per unit mass. The diffusive effects in the density equation are omitted in set (13.2) because they are not considered here.

Set (13.2) makes the so-called *Boussinesq approximation*, discussed in Section 4.18, in which the density variations are neglected everywhere except in the gravity term. Along with other restrictions, it assumes that the vertical scale of the motion is less than the "scale height" of the medium c^2/g, where c is the speed of sound. This assumption is very good in the ocean, in which $c^2/g \sim 200$ km. In the atmosphere it is less applicable, because $c^2/g \sim 10$ km. Under the Boussinesq approximation, the principle of mass conservation is expressed by $\nabla\cdot\mathbf{u} = 0$. In contrast, the density equation $D\rho/Dt = 0$ follows from the nondiffusive heat equation $DT/Dt = 0$ and an incompressible equation of state of the form $\delta\rho/\rho_0 = -\alpha\delta T$. (If the density is determined by the concentration S of a constituent, say the water vapor in the atmosphere or the salinity in the ocean, then $D\rho/Dt = 0$ follows from the nondiffusive conservation equation for the constituent in the form $DS/Dt = 0$, plus the incompressible equation of state $\delta\rho/\rho_0 = \beta\delta S$.)

The equations can be written in terms of the pressure and density *perturbations* from a state of rest. In the absence of any motion, suppose the density and pressure have the vertical distributions $\overline{\rho}(z)$ and $\overline{p}(z)$, where the z-axis is taken vertically upward. As this state is hydrostatic, we must have

$$\frac{d\overline{p}}{dz} = -\overline{\rho}g. \tag{13.3}$$

In the presence of a flow field $\mathbf{u}(\mathbf{x},t)$, we can write the density and pressure as

$$\begin{aligned} \rho(\mathbf{x},t) &= \overline{\rho}(z) + \rho'(\mathbf{x},t), \\ p(\mathbf{x},t) &= \overline{p}(z) + p'(\mathbf{x},t), \end{aligned} \tag{13.4}$$

where ρ' and p' are the changes from the state of rest. With this substitution, the first two terms on the right-hand side of the momentum equation in (13.2) give

$$-\frac{1}{\rho_0}\nabla p - \frac{g\rho}{\rho_0}\mathbf{e}_z = -\frac{1}{\rho_0}\nabla(\overline{p}+p') - \frac{g}{\rho_0}(\overline{\rho}+\rho')\mathbf{e}_z = -\frac{1}{\rho_0}\left[\frac{d\overline{p}}{dz}\mathbf{e}_z + \nabla p'\right] - \frac{g}{\rho_0}(\overline{\rho}+\rho')\mathbf{e}_z.$$

Subtracting the hydrostatic state (13.3), this becomes

$$-\frac{1}{\rho_0}\nabla p - \frac{g\rho}{\rho_0}\mathbf{e}_z = -\frac{1}{\rho_0}\nabla p' - \frac{g\rho'}{\rho_0}\mathbf{e}_z,$$

which shows that we can replace p and ρ in (13.2) by the perturbation quantities p' and ρ'.

The friction force per unit mass **F** in equation (13.2) needs to be related to the velocity field. From Section 4.4, the friction force is given by $F_i = \partial\tau_{ij}/\partial x_j$, where τ_{ij} is the viscous stress tensor. The stress in a laminar flow is caused by the molecular exchanges of momentum. From (4.35), the viscous stress tensor in an isotropic incompressible medium in laminar

flow is given by $\mu(\partial u_i/\partial x_j + \partial u_j/\partial x_i)$. In large-scale geophysical flows, however, the frictional forces are provided by turbulent momentum exchange and viscous effects are negligible. The complexity of turbulent behavior makes it impossible to relate the stress to the velocity field in a simple way. To proceed, then, we adopt the eddy viscosity hypothesis (12.94), which sets the turbulent stress proportional to the velocity gradient field.

Geophysical media are in the form of shallow stratified layers, in which the vertical velocities are much smaller than horizontal velocities. This means that the exchange of momentum across a horizontal surface is much weaker than that across a vertical surface. We expect then that the vertical eddy viscosity ν_{v} is much smaller than the horizontal eddy viscosity ν_{H}, and we assume that the turbulent stress components have the form:

$$\begin{aligned}
\tau_{xz} &= \tau_{zx} = \rho\nu_{\mathrm{v}}\frac{\partial u}{\partial z} + \rho\nu_{\mathrm{H}}\frac{\partial w}{\partial x},\\
\tau_{yz} &= \tau_{zy} = \rho\nu_{\mathrm{v}}\frac{\partial v}{\partial z} + \rho\nu_{\mathrm{H}}\frac{\partial w}{\partial y},\\
\tau_{xy} &= \tau_{yx} = \rho\nu_{\mathrm{H}}\left(\frac{\partial u}{\partial y} + \frac{\partial v}{\partial x}\right),\\
\tau_{xx} = 2\rho\nu_{\mathrm{H}}\frac{\partial u}{\partial x}, &\quad \tau_{yy} = 2\rho\nu_{\mathrm{H}}\frac{\partial v}{\partial y}, \quad \tau_{zz} = 2\rho\nu_{\mathrm{v}}\frac{\partial w}{\partial z}.
\end{aligned} \tag{13.5}$$

The difficulty with set (13.5) is that the expressions for τ_{xz} and τ_{yz} depend on the fluid *rotation* in the vertical plane and not just the deformation. In Section 4.5, we saw that a requirement for a constitutive equation is that the stresses should be independent of fluid rotation and should depend only on the deformation. Therefore, τ_{xz} should depend only on the combination $(\partial u/\partial z + \partial w/\partial x)$, whereas the expression in (13.5) depends on both deformation and rotation. A tensorially correct geophysical treatment of the frictional terms is discussed, for example, in Kamenkovich (1967). However, the assumed form (13.5) leads to a simple formulation for viscous effects, as we shall see shortly. As the eddy viscosity assumption is of questionable validity (which Pedlosky [1971] describes as a "rather disreputable and desperate attempt"), there does not seem to be any purpose in formulating the stress-strain relation in more complicated ways merely to obey the requirement of invariance with respect to rotation.

With the assumed form for the turbulent stress, the components of the frictional force $F_i = \partial\tau_{ij}/\partial x_j$ become:

$$\begin{aligned}
F_x &= \frac{\partial\tau_{xx}}{\partial x} + \frac{\partial\tau_{xy}}{\partial y} + \frac{\partial\tau_{xz}}{\partial z} = \nu_{\mathrm{H}}\left(\frac{\partial^2 u}{\partial x^2} + \frac{\partial^2 u}{\partial y^2}\right) + \nu_{\mathrm{v}}\frac{\partial^2 u}{\partial z^2},\\
F_y &= \frac{\partial\tau_{yx}}{\partial x} + \frac{\partial\tau_{yy}}{\partial y} + \frac{\partial\tau_{yz}}{\partial z} = \nu_{\mathrm{H}}\left(\frac{\partial^2 v}{\partial x^2} + \frac{\partial^2 v}{\partial y^2}\right) + \nu_{\mathrm{v}}\frac{\partial^2 v}{\partial z^2},\\
F_z &= \frac{\partial\tau_{zx}}{\partial x} + \frac{\partial\tau_{zy}}{\partial y} + \frac{\partial\tau_{zz}}{\partial z} = \nu_{\mathrm{H}}\left(\frac{\partial^2 w}{\partial x^2} + \frac{\partial^2 w}{\partial y^2}\right) + \nu_{\mathrm{v}}\frac{\partial^2 w}{\partial z^2}.
\end{aligned} \tag{13.6}$$

Estimates of the eddy coefficients vary greatly. Typical suggested values are $\nu_v \sim 10\ m^2/s$ and $\nu_H \sim 10^5\ m^2/s$ for the lower atmosphere, and $\nu_v \sim 0.01\ m^2/s$ and $\nu_H \sim 100\ m^2/s$ for the upper ocean. In comparison, the molecular values are $\nu = 1.5 \times 10^{-5}\ m^2/s$ for air and $\nu = 10^{-6}\ m^2/s$ for water.

13.4. APPROXIMATE EQUATIONS FOR A THIN LAYER ON A ROTATING SPHERE

The atmosphere and the ocean are very thin layers in which the depth scale of flow is a few kilometers, whereas the horizontal scale is of the order of hundreds, or even thousands, of kilometers. The trajectories of fluid elements are nearly horizontal while vertical velocities are much smaller than horizontal velocities. In fact, the continuity equation suggests that the scale of the vertical velocity W is related to that of the horizontal velocity U by

$$\frac{W}{U} \sim \frac{H}{L},$$

where H is the depth scale and L is the horizontal length scale. Stratification and Coriolis effects usually constrain the vertical velocity to be even smaller than UH/L.

Large-scale geophysical flow problems should be solved using spherical polar coordinates. If, however, the horizontal length scales are much smaller than the radius of the earth ($= 6371$ km), then the curvature of the earth can be ignored, and the motion can be studied by adopting a *local* Cartesian system on a *tangent plane* (Figure 13.3). On this plane we take an xyz

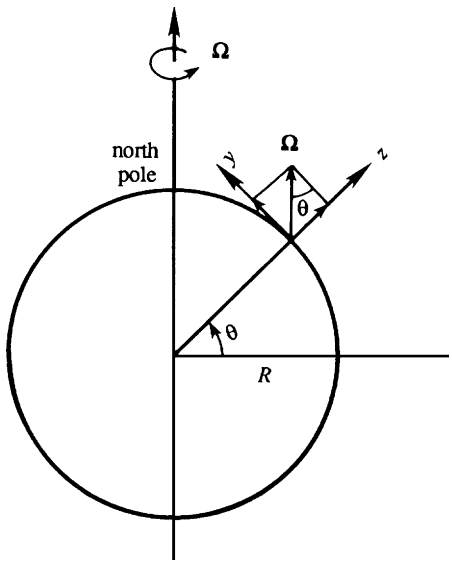

FIGURE 13.3 Local Cartesian coordinates. The x-axis points into the plane of the paper. The y-axis is tangent to the earth's surface and points toward the north pole. The z-axis is vertical, opposing gravity. The earth's angular rotation vector has positive y and z components in the northern hemisphere.

coordinate system, with x increasing eastward, y northward, and z upward. The corresponding velocity components are u (eastward), v (northward), and w (upward).

The earth rotates at a rate,

$$\Omega = 2\pi \, rad/day = 0.73 \times 10^{-4} \, s^{-1},$$

around the polar axis, in a counterclockwise sense looking from above the north pole. From Figure 13.3, the components of angular velocity of the earth in the local Cartesian system are $\mathbf{\Omega} = (\Omega_x, \Omega_y, \Omega_z) = (0, \Omega\cos\theta, \Omega\sin\theta)$, where θ is the latitude. The Coriolis acceleration is therefore:

$$2\mathbf{\Omega} \times \mathbf{u} = \begin{vmatrix} \mathbf{e}_x & \mathbf{e}_y & \mathbf{e}_z \\ 0 & 2\Omega\cos\theta & 2\Omega\sin\theta \\ u & v & w \end{vmatrix} = 2\Omega\left[\mathbf{e}_x\left(w\cos\theta - v\sin\theta\right) + \mathbf{e}_y u\sin\theta - \mathbf{e}_z u\cos\theta\right].$$

In the term multiplied by $\mathbf{e}_x$ we can use the condition $w\cos\theta \ll v\sin\theta$, because the thin-sheet approximation requires that $w \ll v$. The three components of the Coriolis acceleration are therefore

$$2\mathbf{\Omega} \times \mathbf{u} \cong (-2\Omega v\sin\theta, \, 2\Omega u\sin\theta, -2\Omega u\cos\theta) = (-fv, fu, -2\Omega u\cos\theta), \tag{13.7}$$

where we have defined

$$f = 2\Omega\sin\theta \tag{13.8}$$

to be twice the *vertical* component of $\mathbf{\Omega}$. As vorticity is twice the angular velocity, f is called the *planetary vorticity*. More commonly, f is referred to as the *Coriolis parameter*, or the *Coriolis frequency*. It is positive in the northern hemisphere and negative in the southern hemisphere, varying from $\pm 1.45 \times 10^{-4}$ s^{-1} at the poles to zero at the equator. This makes sense, since a person standing at the north pole spins around himself in a counterclockwise sense at a rate Ω, whereas a person standing at the equator does not spin around himself but simply translates. The quantity,

$$T_i = 2\pi/f,$$

is called the *inertial period*, for reasons that will be clear in Section 13.11; it does refer to a component of the vector.

The vertical component of the Coriolis force, namely $-2\Omega u\cos\theta$, is generally negligible compared to the dominant terms in the vertical equation of motion, namely $g\rho'/\rho_0$ and $\rho_0^{-1}(\partial p'/\partial z)$. Using (13.6), (13.7), and (13.8), the equations of motion (13.2) reduce to:

$$\begin{aligned} \frac{Du}{Dt} - fv &= -\frac{1}{\rho_0}\frac{\partial p}{\partial x} + \nu_H\left(\frac{\partial^2 u}{\partial x^2} + \frac{\partial^2 u}{\partial y^2}\right) + \nu_v\frac{\partial^2 u}{\partial z^2}, \\ \frac{Dv}{Dt} + fu &= -\frac{1}{\rho_0}\frac{\partial p}{\partial y} + \nu_H\left(\frac{\partial^2 v}{\partial x^2} + \frac{\partial^2 v}{\partial y^2}\right) + \nu_v\frac{\partial^2 v}{\partial z^2}, \\ \frac{Dw}{Dt} &= -\frac{1}{\rho_0}\frac{\partial p}{\partial z} - \frac{g\rho}{\rho_0} + \nu_H\left(\frac{\partial^2 w}{\partial x^2} + \frac{\partial^2 w}{\partial y^2}\right) + \nu_v\frac{\partial^2 w}{\partial z^2}. \end{aligned} \tag{13.9}$$

These are the equations of motion for a thin shell on a rotating earth. Note that only the *vertical* component of the earth's angular velocity appears as a consequence of the flatness of the fluid trajectories.

f-Plane Model

The Coriolis parameter $f = 2\Omega \sin \theta$ varies with latitude θ. However, this variation is important only for phenomena having very long time scales (several weeks) or very long length scales (thousands of kilometers). For many purposes we can assume f to be a constant, say $f_0 = 2\Omega \sin \theta_0$, where θ_0 is the central latitude of the region under study. A model using a constant Coriolis parameter is called an *f-plane model*.

β-Plane Model

The variation of f with latitude can be approximately represented by expanding f in a Taylor series about the central latitude θ_0:

$$f = f_0 + \beta y, \tag{13.10}$$

where

$$\beta \equiv \left(\frac{df}{dy}\right)_{\theta_0} = \left(\frac{df}{d\theta}\frac{d\theta}{dy}\right)_{\theta_0} = \frac{2\Omega \cos \theta_0}{R}.$$

Here, we have used $f = 2\Omega \sin \theta$ and $d\theta/dy = 1/R$, where the radius of the earth is nearly $R = 6371$ km. A model that takes into account the variation of the Coriolis parameter in the simplified form $f = f_0 + \beta y$, with β as constant, is called a *β-plane model*.

13.5. GEOSTROPHIC FLOW

Consider quasi-steady, large-scale motions in the atmosphere or the ocean, away from boundaries. For these flows an excellent approximation for the horizontal equilibrium is a balance between the Coriolis force and the pressure gradient:

$$-fv = -\frac{1}{\rho_0}\frac{\partial p}{\partial x}, \quad \text{and} \quad fu = -\frac{1}{\rho_0}\frac{\partial p}{\partial y}. \tag{13.11, 13.12}$$

Here we have neglected the nonlinear acceleration terms, which are of order U^2/L, in comparison to the Coriolis force $\sim fU$ (U is the horizontal velocity scale, and L is the horizontal length scale). The ratio of the nonlinear term to the Coriolis term is called the *Rossby number*:

$$\text{Rossby number} = \frac{\text{Nonlinear acceleration}}{\text{Coriolis force}} \sim \frac{U^2/L}{fU} = \frac{U}{fL} = Ro. \tag{13.13}$$

For a typical atmospheric value of $U \sim 10$ m/s, $f \sim 10^{-4}$ s^{-1}, and $L \sim 1000$ km, the Rossby number turns out to be 0.1. The Rossby number is even smaller for many flows in the ocean, so that the neglect of nonlinear terms is justified for many flows.

The balance of forces represented by (13.11), in which the horizontal pressure gradients are balanced by Coriolis forces, is called a *geostrophic balance*. In such a system the velocity distribution can be determined from a measured distribution of the pressure field. The geostrophic equilibrium breaks down near the equator (within a latitude belt of $\pm 3^\circ$), where f becomes small. It also breaks down if the frictional effects or unsteadiness become important.

Velocities in a geostrophic flow are perpendicular to the horizontal pressure gradient. This is because (13.11) implies that $\mathbf{u}\cdot\nabla p = 0$, that is:

$$(u\mathbf{e}_x + v\mathbf{e}_y)\cdot\nabla p = \frac{1}{\rho_0 f}\left(-\mathbf{e}_x\frac{\partial p}{\partial y} + \mathbf{e}_y\frac{\partial p}{\partial x}\right)\cdot\left(\mathbf{e}_x\frac{\partial p}{\partial x} + \mathbf{e}_y\frac{\partial p}{\partial y}\right) = 0.$$

Thus, the horizontal velocity is *along*, and not across, the lines of constant pressure. If f is regarded as constant, then the geostrophic balance (13.11) shows that $p/f\rho_0$ can be regarded as a stream function. The isobars on a weather map are therefore nearly the streamlines of the flow.

Figure 13.4 shows the geostrophic flow around low- and high-pressure centers in the northern hemisphere. Here the Coriolis force acts to the right of the velocity vector. This requires the flow to be counterclockwise (viewed from above) around a low-pressure region and clockwise around a high-pressure region. The sense of circulation is opposite in the southern hemisphere, where the Coriolis force acts to the left of the velocity vector. (Frictional forces become important at lower levels in the atmosphere and result in a flow partially *across* the isobars. This will be discussed in Section 13.7, where it is shown that flow around a low-pressure center spirals *inward* due to frictional effects.)

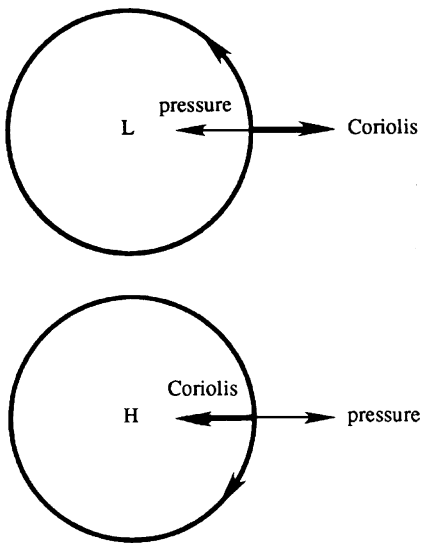

FIGURE 13.4 Circular geostrophic flow around ideal low- and high-pressure centers in the northern hemisphere. The pressure force ($-\nabla p$) is indicated by a thin arrow, and the Coriolis force is indicated by a thick arrow.

The flow along isobars at first surprises a reader unfamiliar with the effects of the Coriolis force. A question commonly asked is: How is such a motion set up? A typical manner of establishment of such a flow is as follows. Consider a horizontally converging flow in the surface layer of the ocean. The convergent flow sets up the sea surface in the form of a gentle hill, with the sea surface dropping away from the center of the hill. A fluid particle starting to move down the hill is deflected to the right in the northern hemisphere, and a steady state is reached when the particle finally moves *along* the isobars.

Thermal Wind

In the presence of a *horizontal* gradient of density, the geostrophic velocity develops a *vertical* shear. This is easy to demonstrate from an analysis of the geostrophic and hydrostatic balance using (13.11), (13.12), and

$$0 = -\frac{\partial p}{\partial z} - g\rho. \tag{13.14}$$

Eliminating p between (13.11) and (13.14), and also between equations (13.12) and (13.14), we obtain, respectively,

$$\frac{\partial v}{\partial z} = -\frac{g}{\rho_0 f}\frac{\partial \rho}{\partial x}, \quad \text{and} \quad \frac{\partial u}{\partial z} = \frac{g}{\rho_0 f}\frac{\partial \rho}{\partial y}. \tag{13.15}$$

Meteorologists call these the *thermal wind* equations because they give the vertical variation of wind from measurements of horizontal temperature (and pressure) gradients. The thermal wind is a baroclinic phenomenon, because the surfaces of constant p and ρ do not coincide.

Taylor-Proudman Theorem

A striking phenomenon occurs in the geostrophic flow of a *homogeneous* fluid. It can only be observed in a laboratory experiment because stratification effects cannot be avoided in natural flows. Consider then a laboratory experiment in which a tank of fluid is steadily rotated at a high angular speed Ω and a solid body is moved slowly along the bottom of the tank. The purpose of making Ω large and the movement of the solid body slow is to make the Coriolis force much larger than the advective acceleration terms, which must be made negligible for geostrophic equilibrium. Away from the frictional effects of boundaries, the balance is therefore geostrophic in the horizontal and hydrostatic in the vertical. Setting $f = 2\Omega$ in (13.11) and (13.12) produces

$$-2\Omega v = -\frac{1}{\rho}\frac{\partial p}{\partial x} \quad \text{and} \quad -2\Omega u = -\frac{1}{\rho}\frac{\partial p}{\partial y}. \tag{13.16, 13.17}$$

It is useful to define an Ekman number as the ratio of viscous to Coriolis forces (per unit volume):

$$\text{Ekman number} = \frac{\text{viscous force}}{\text{Coriolis force}} = \frac{\rho \nu U/L^2}{\rho f U} = \frac{\nu}{fL^2} = E. \tag{13.18}$$

Under the circumstances already described here, both Ro and E are small.

Elimination of p by cross differentiation of the horizontal momentum equations (13.16) and (13.17) gives

$$2\Omega\left(\frac{\partial v}{\partial y}+\frac{\partial u}{\partial x}\right) = 0.$$

Using the continuity equation, this gives

$$\frac{\partial w}{\partial z} = 0. \tag{13.19}$$

Also, differentiating (13.16) and (13.17) with respect to z, and using (13.14), we obtain

$$\frac{\partial v}{\partial z} = \frac{\partial u}{\partial z} = 0. \tag{13.20}$$

Taken together, (13.19) and (13.20) imply

$$\partial \mathbf{u}/\partial z = 0. \tag{13.21}$$

Thus, the fluid velocity cannot vary in the direction of Ω. In other words, steady slow motions in a rotating, homogeneous, inviscid fluid are two dimensional. This is the *Taylor-Proudman theorem*, first derived by Proudman in 1916 and demonstrated experimentally by Taylor soon afterward.

In Taylor's experiment, a tank was made to rotate as a solid body, and a small cylinder was slowly dragged along the bottom of the tank (Figure 13.5). Dye was introduced from point A above the cylinder and directly ahead of it. In a nonrotating fluid the water would pass over the top of the moving cylinder. In the rotating experiment, however, the dye divides at a point S, as if it had been blocked by a vertical extension of the cylinder, and flows around this *imaginary* cylinder, called the *Taylor column*. Dye released from a point B within the Taylor column remained there and moved with the cylinder. The conclusion was that the flow outside the upward extension of the cylinder is the same as if the cylinder extended across the entire water depth and that a column of water directly above the cylinder moves with it. The motion is two dimensional, although the solid body does not extend across the entire water depth. Taylor did a second experiment, in which he dragged a solid body *parallel* to the axis of rotation. In accordance with $\partial w/\partial z = 0$, he observed that a column of fluid is pushed ahead. The lateral velocity components u and v were zero. In both of these experiments, there are shear layers at the edge of the Taylor column.

In summary, Taylor's experiment established the following striking fact for steady inviscid motion of homogeneous fluid in a strongly rotating system: Bodies moving either parallel or perpendicular to the axis of rotation carry along with their motion a so-called Taylor column of fluid, oriented parallel to the axis of rotation. The phenomenon is analogous to the horizontal *blocking* caused by a solid body (say a mountain) in a strongly stratified system, shown in Figure 7.30.

13.6. EKMAN LAYER AT A FREE SURFACE

In the preceding section, we discussed a steady linear inviscid motion expected to be valid away from frictional boundary layers. We shall now examine the motion within frictional

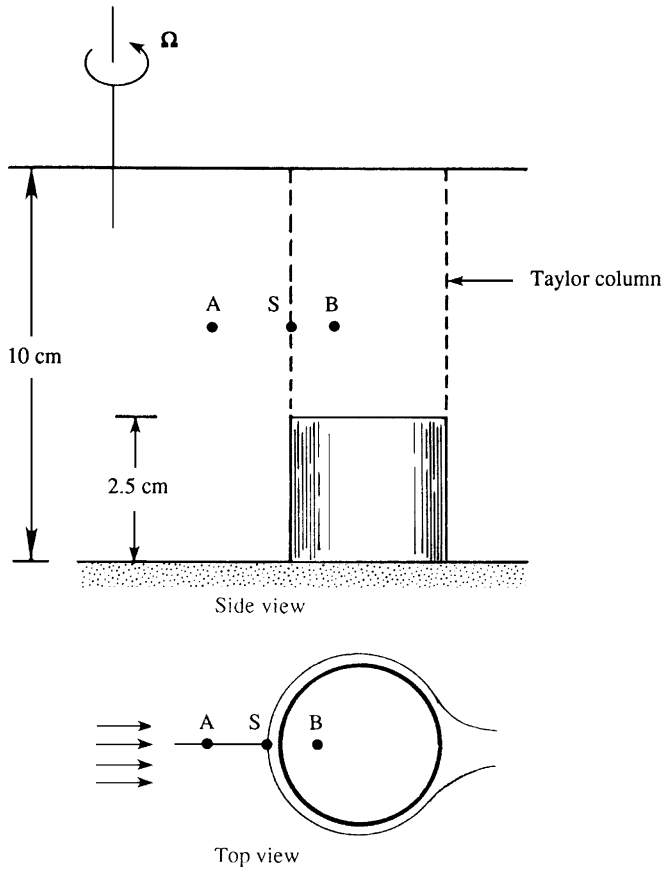

FIGURE 13.5 Taylor's experiment in a strongly rotating flow of a homogeneous fluid. When the short cylinder is moved toward the axis of rotation, an extension of the cylinder forms in the fluid above it. Dye released above the cylinder at point A flows around the extension of cylinder as if it were a solid object. Dye released above the cylinder at point B follows the motion of the short cylinder.

layers over horizontal surfaces. In viscous flows unaffected by Coriolis forces and pressure gradients, the only term which can balance the viscous force is either the time derivative $\partial \mathbf{u}/\partial t$ or the advection $\mathbf{u}\cdot\nabla\mathbf{u}$. The balance of $\partial \mathbf{u}/\partial t$ and the viscous force gives rise to a viscous layer whose thickness increases with time, as in the suddenly accelerated plate discussed in Section 8.7. The balance of $\mathbf{u}\cdot\nabla\mathbf{u}$ and the viscous force give rise to a viscous layer whose thickness increases in the direction of flow, as in the boundary layer over a semi-infinite plate discussed in Sections 9.3 through 9.5. In a rotating flow, however, we can have a balance between the Coriolis and the viscous forces, and the thickness of the viscous layer can be invariant in time and space. Two examples of such layers are given in this and the following sections.

Consider first the case of a frictional layer near the free surface of the ocean, which is acted on by a wind stress τ in the x-direction. We shall not consider how the flow adjusts to the

steady state but examine only the steady solution. We shall assume that the horizontal pressure gradients are zero and that the field is horizontally homogeneous. From (13.9), the horizontal equations of motion for flow within the ocean are:

$$-fv = \nu_v \frac{d^2u}{dz^2} \quad \text{and} \quad fu = \nu_v \frac{d^2v}{dz^2}. \tag{13.22, 13.23}$$

Defining $z = 0$ on the surface of the ocean, the boundary conditions are:

$$\rho\nu_v(du/dz) = \tau \text{ at } z = 0,\ dv/dz = 0 \text{ at } z = 0, \text{ and } u, v \to 0 \text{ as } z \to \infty. \tag{13.24, 13.25, 13.26}$$

Multiplying equation (13.23) by the imaginary root, $i = \sqrt{-1}$, and adding equation (13.22), we obtain

$$\frac{d^2V}{dz^2} = \frac{if}{\nu_v} V, \tag{13.27}$$

where we have defined the *complex velocity*

$$V \equiv u + iv.$$

The solution of (13.27) is

$$V = A\, e^{(1+i)z/\delta} + B\, e^{-(1+i)z/\delta}, \text{ where } \delta = \sqrt{2\nu_v/f}. \tag{13.28, 13.29}$$

The constant B is zero because the field must remain finite as $z \to -\infty$, and δ is the thickness of the *Ekman layer*. The surface boundary conditions (13.24) and (13.25) can be combined as $\rho\nu_v(dV/dz) = \tau$ at $z = 0$, from which (13.28) gives

$$A = \frac{\tau\delta(1-i)}{2\rho\nu_v}.$$

Substitution of this into (13.28) gives the velocity components:

$$u = \frac{\tau/\rho}{\sqrt{f\nu_v}} e^{z/\delta} \cos\left(-\frac{z}{\delta} + \frac{\pi}{4}\right),$$

$$v = -\frac{\tau/\rho}{\sqrt{f\nu_v}} e^{z/\delta} \sin\left(-\frac{z}{\delta} + \frac{\pi}{4}\right).$$

The Swedish oceanographer Ekman worked out this solution in 1905. The solution is shown in Figure 13.6 for the case of the northern hemisphere, in which f is positive. The velocities at various depths within the ocean are plotted in Figure 13.6a where each arrow represents the velocity vector at a certain depth. Such a plot of v versus u is sometimes called a *hodograph*. The vertical distributions of u and v are shown in Figure 13.6b. The hodograph shows that the surface velocity is deflected 45° to the right of the applied wind stress. (In the southern hemisphere the deflection is to the left of the surface stress.) The velocity vector rotates clockwise (looking down) with depth, and the magnitude exponentially decays with an e-folding scale of δ, the Ekman layer thickness. The tips of the velocity vector at various depths form a spiral, called the *Ekman spiral*.

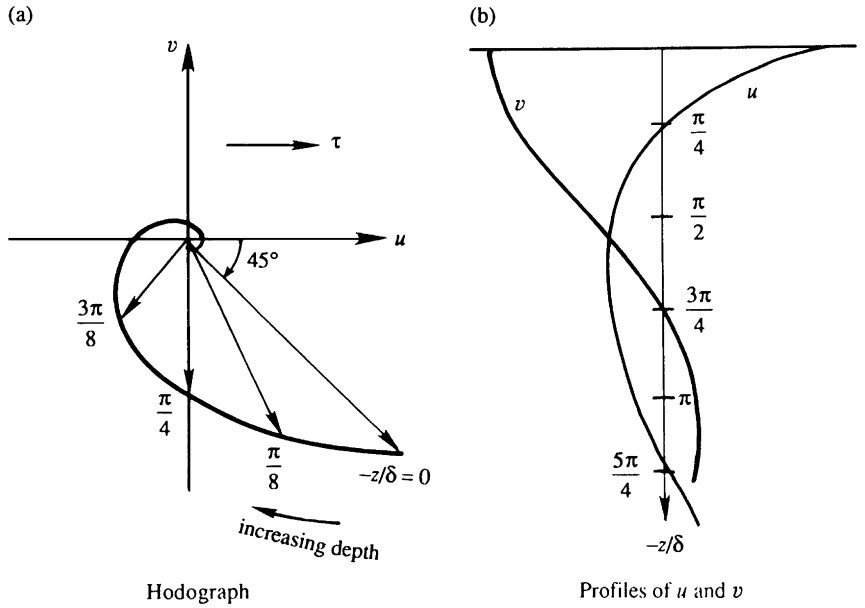

FIGURE 13.6 Ekman layer below a water surface on which a shear stress τ is applied in the x-direction. The left panel (a) shows the horizontal fluid velocity components (u, v) at various depths; values of $-z/\delta$ are indicated along the curve traced out by the tip of the velocity vector. The flow speed is highest near the surface. The right panel (b) shows vertical distributions of u and v. Here, the Coriolis force produces significant depth dependence in the fluid velocity even though τ is constant and unidirectional.

The components of the volume transport in the Ekman layer are:

$$\begin{aligned} \int_{-\infty}^{0} u\,dz &= 0, \\ \int_{-\infty}^{0} v\,dz &= -\frac{\tau}{\rho f}. \end{aligned} \tag{13.30}$$

This shows that the *net transport is to the right of the applied stress and is independent of* ν_v. In fact, the result $\int v\,dz = -\tau/f\rho$ follows directly from a vertical integration of the equation of motion in the form $-\rho f v = d\tau/dz$ so that the result does not depend on the eddy viscosity assumption. The fact that the transport is to the right of the applied stress makes sense because then the net (depth-integrated) Coriolis force, directed to the right of the depth-integrated transport, can balance the wind stress.

The horizontal uniformity assumed in the solution is not a serious limitation. Since Ekman layers near the ocean surface have a thickness (~50 m) much smaller than the scale of horizontal variation ($L > 100$ km), the solution is still locally applicable. The assumed absence of a horizontal pressure gradient can also be reconsidered. Because of the thinness of the layer, any imposed horizontal pressure gradient remains constant across the layer. The presence of a horizontal pressure gradient merely adds a depth-independent geostrophic velocity to the Ekman solution. Suppose the sea surface slopes

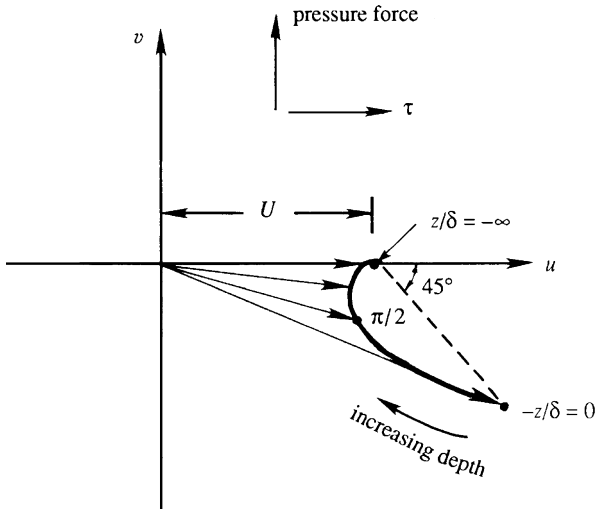

FIGURE 13.7 Ekman layer at a free surface in the presence of a pressure gradient. The geostrophic velocity forced by the pressure gradient is U. The flow profile in this case is the sum of U and the profile shown in Figure 13.6.

down to the north, so that there is a pressure force acting northward throughout the Ekman layer and below (Figure 13.7). This means that at the bottom of the Ekman layer ($z/\delta \to -\infty$) there is a geostrophic velocity U to the right of the pressure force. The surface Ekman spiral forced by the wind stress joins smoothly to this geostrophic velocity as $z/\delta \to -\infty$.

Pure Ekman spirals are not observed in the surface layer of the ocean, mainly because the assumptions of constant eddy viscosity and steadiness are particularly restrictive. When the flow is averaged over a few days, however, several instances have been found in which the current does look like a spiral. One such example is shown in Figure 13.8.

Explanation in Terms of Vortex Tilting

We have seen in previous chapters that the thickness of a viscous layer usually grows in a nonrotating flow, either in time or in the direction of flow. The Ekman solution, in contrast, results in a viscous layer that does not grow either in time or space. This can be explained by examining the vorticity equation (Pedlosky, 1987). The vorticity components in the x- and y-directions are:

$$\omega_x = \frac{\partial w}{\partial y} - \frac{\partial v}{\partial z} = -\frac{dv}{dz},$$

$$\omega_y = \frac{\partial u}{\partial z} - \frac{\partial w}{\partial x} = \frac{du}{dz},$$

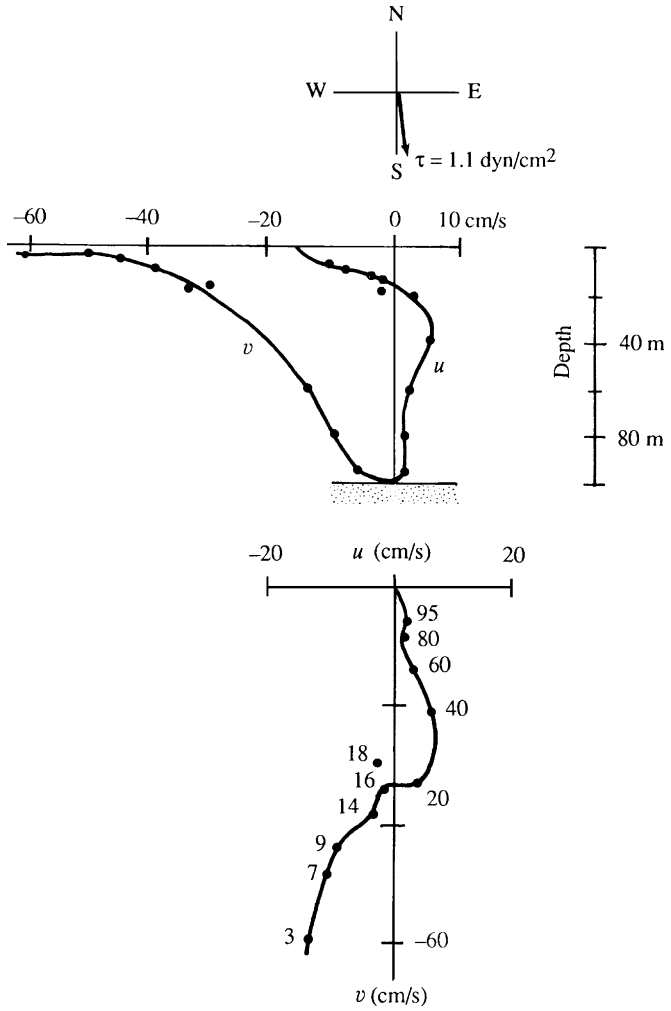

FIGURE 13.8 An observed velocity distribution near the coast of Oregon. Velocity is averaged over 7 days. Wind stress had a magnitude of 1.1 dyn/cm^2 and was directed nearly southward, as indicated at the top of the figure. The upper panel shows vertical distributions of u and v, and the lower panel shows the hodograph in which depths are indicated in meters. The hodograph is similar to that of a surface Ekman layer (of depth 16 m) lying over the bottom Ekman layer (extending from a depth of 16 m to the ocean bottom). *P. Kundu, in* Bottom Turbulence, *J. C. J. Nihoul, ed., Elsevier, 1977; reprinted with the permission of Jacques C. J. Nihoul.*

where we have used $w = 0$. Using these, the z-derivative of the equations of motion (13.22) and (13.23) gives:

$$\begin{aligned} -f\frac{dv}{dz} &= \nu_v \frac{d^2\omega_y}{dz^2}, \\ -f\frac{du}{dz} &= \nu_v \frac{d^2\omega_x}{dz^2}. \end{aligned} \tag{13.31}$$

The right sides of these equations represent diffusion of vorticity. Without Coriolis forces this diffusion would cause a thickening of the viscous layer. The presence of planetary rotation, however, means that vertical fluid lines coincide with the planetary vortex lines. The tilting of vertical fluid lines, represented by terms on the left-hand sides of equations (13.31), then causes a rate of change of the horizontal component of vorticity that just cancels the diffusion term.

13.7. EKMAN LAYER ON A RIGID SURFACE

Consider a steady viscous layer on a solid surface in a rotating flow that is independent of the horizontal coordinates x and y. This can be the atmospheric boundary layer over the solid earth or the boundary layer over the ocean bottom. We assume that at large distances from the surface the velocity is toward the x-direction and has a magnitude U. Viscous forces are negligible far from the wall, so that the Coriolis force can be balanced only by a pressure gradient:

$$fU = -\frac{1}{\rho}\frac{dp}{dy}. \tag{13.32}$$

This simply states that the flow outside the viscous layer is in geostrophic balance, U being the geostrophic velocity. For our assumed case of positive U and f, we must have $dp/dy < 0$, so that the pressure falls with y—that is, the pressure force is directed along the positive y direction, resulting in a geostrophic flow U to the right of the pressure force in the northern hemisphere. The horizontal pressure gradient remains constant within the thin boundary layer.

Near the solid surface friction forces are important, so that the balance within the boundary layer is

$$-fv = \nu_v \frac{d^2u}{dz^2} \quad \text{and} \quad fu = \nu_v \frac{d^2v}{dz^2} + fU, \tag{13.33, 13.34}$$

where we have replaced $-\rho^{-1}(dp/dy)$ by fU in accordance with (13.32). The boundary conditions are:

$$u = U, \quad v = 0 \quad \text{as } z \to \infty, \tag{13.35}$$

$$u = 0, \quad v = 0 \quad \text{at } z = 0, \tag{13.36}$$

where z is taken vertically upward from the solid surface. Multiplying equation (13.34) by i and adding equation (13.33), the equations of motion become

$$\frac{d^2V}{dz^2} = \frac{if}{\nu_v}(V - U), \tag{13.37}$$

where we have again used the complex velocity $V \equiv u + iv$. The boundary conditions (13.35) and (13.36) in terms of the complex velocity are:

$$V = U \quad \text{as } z \to \infty, \tag{13.38}$$

$$V = 0 \quad \text{at } z = 0. \tag{13.39}$$

The particular solution of (13.37) is $V = U$. The total solution is, therefore,

$$V = A\,e^{-(1+i)z/\delta} + B\,e^{(1+i)z/\delta} + U, \tag{13.40}$$

where $\delta \equiv \sqrt{2\nu_v/f}$, as before. To satisfy (13.38), we must have $B = 0$. Condition (13.39) gives $A = -U$. The velocity components then become:

$$\begin{aligned} u &= U\left[1 - e^{-z/\delta}\cos\left(z/\delta\right)\right], \\ v &= Ue^{-z/\delta}\sin\left(z/\delta\right). \end{aligned} \tag{13.41}$$

According to (13.41), the tip of the velocity vector describes a spiral for various values of z (Figure 13.9a). As with the Ekman layer at a free surface, the frictional effects are confined within a layer of thickness $\delta = \sqrt{2\nu_v/f}$, which increases with ν_v and decreases with the rotation rate f. Interestingly, the layer thickness is independent of the magnitude of the free-stream velocity U; this behavior is quite different from that of a steady nonrotating boundary layer on a semi-infinite plate (the Blasius solution of Section 9.3) in which the thickness is proportional to $1/\sqrt{U}$.

Figure 13.9b shows the vertical distribution of the velocity components. Far from the wall the velocity is entirely in the x-direction, and the Coriolis force balances the pressure gradient. As the wall is approached, frictional effects decrease u and the associated Coriolis force, so that the pressure gradient (which is independent of z) forces a component v in the direction of the pressure force. Using (13.41), the net transport in the Ekman layer normal to the uniform stream outside the layer is

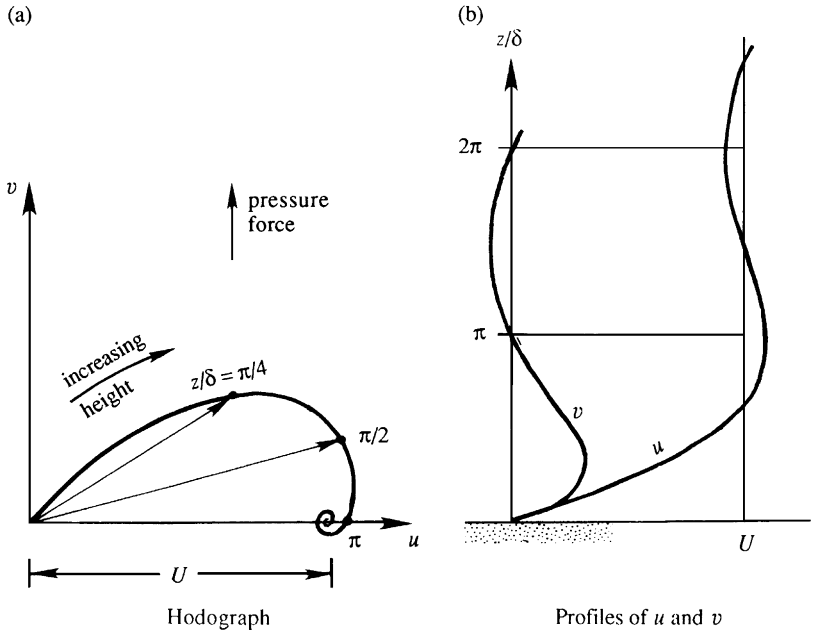

FIGURE 13.9 Ekman layer above a rigid surface for a steady outer-flow velocity of U (parallel to the x-axis). The left panel shows velocity vectors at various heights; values of z/δ are indicated along the curve traced out by the tip of the velocity vectors. The right panel shows vertical distributions of u and v.

$$\int_0^\infty v\,dz = U\left[\frac{\nu_v}{2f}\right]^{1/2} = \frac{1}{2}U\delta,$$

which is directed to the *left* of the free-stream velocity, in the direction of the pressure force.

If the atmosphere were in laminar motion, ν_v would be equal to its molecular value for air, and the Ekman layer thickness at a latitude of 45° (where $f \simeq 10^{-4}\,s^{-1}$) would be $\approx \delta \sim 0.4$ m. The observed thickness of the atmospheric boundary layer is of order 1 km, which implies an eddy viscosity of order $\nu_v \sim 50\ m^2/s$. In fact, Taylor (1915) tried to estimate the eddy viscosity by matching the predicted velocity distributions (13.41) with the observed wind at various heights.

The Ekman layer solution on a solid surface demonstrates that the three-way balance among the Coriolis force, the pressure force, and the frictional force within the boundary layer results in a component of flow directed toward the lower pressure.

The balance of forces within the boundary layer is illustrated in Figure 13.10. The net frictional force on an element is oriented approximately opposite to the velocity vector **u**. It is clear that a balance of forces is possible only if the velocity vector has a component from high to low pressure, as shown. Frictional forces therefore cause the flow around a low-pressure center to spiral *inward*. Mass conservation requires that the inward converging flow rise within a low-pressure system, resulting in cloud formation and rainfall. This is what happens in a *cyclone*, a low-pressure system. In contrast, within a high-pressure system the air sinks as it spirals outward due to frictional effects. The arrival of high-pressure systems therefore brings in clear skies and fair weather, because the sinking air suppresses cloud formation.

Frictional effects, in particular the Ekman transport by surface winds, play a fundamental role in the theory of wind-driven ocean circulation. Possibly the most important result of

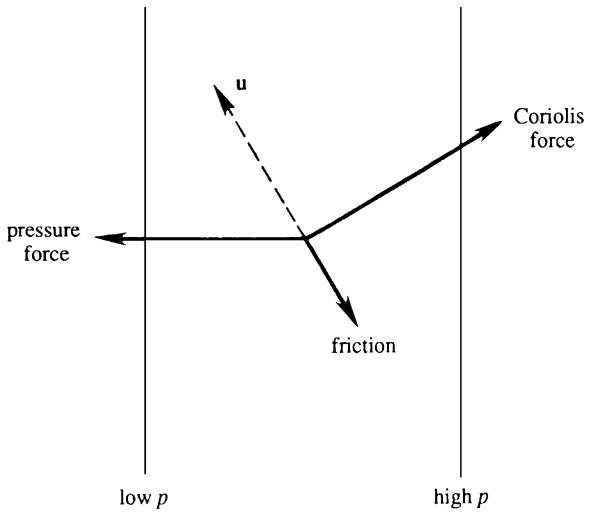

FIGURE 13.10 Balance of forces within an Ekman layer. For steady flow without friction, pressure and Coriolis forces would balance. When friction is added, pressure and Coriolis forces must counteract it. Since friction acts opposite the direction of flow, the velocity **u** must have a component toward lower pressure when friction is present.

such theories was given by Henry Stommel in 1948. He showed that the northward increase of the Coriolis parameter f is responsible for making the currents along western ocean boundaries (e.g., the Gulf Stream in the Atlantic and the Kuroshio in the Pacific) much stronger than the currents on the eastern side. These are discussed in books on physical oceanography and will not be presented here. Instead, we shall now turn our attention to the influence of Coriolis forces on inviscid wave motions.

13.8. SHALLOW-WATER EQUATIONS

Surface and internal gravity waves were discussed in Chapter 7. There the effect of planetary rotation was assumed to be small, which is valid if the frequency ω of the wave is much larger than the Coriolis parameter f. Here, we are considering phenomena slow enough for ω to be comparable to f. Consider surface gravity waves on a shallow layer of homogeneous fluid whose mean depth is H. If we restrict ourselves to wavelengths λ much larger than H, then the vertical velocities are much smaller than the horizontal velocities. In Section 7.2 we determined that the pressure distribution is hydrostatic, and that fluid particles execute a horizontal rectilinear motion that is independent of z. When the effects of planetary rotation are included, the horizontal velocity is still depth independent, although the particle orbits are no longer rectilinear but elliptic on a horizontal plane, as we shall see in the following section.

Consider a layer of fluid of average depth H lying over a flat horizontal bottom (Figure 13.11). Set $z = 0$ on the bottom surface, and let η be the displacement of the free surface. When the pressure on the fluid's surface is set to zero, the pressure at height z from the bottom, which is hydrostatic, is given by

$$p = \rho g(H + \eta - z).$$

The horizontal pressure gradients are therefore

$$\frac{\partial p}{\partial x} = \rho g \frac{\partial \eta}{\partial x}, \quad \frac{\partial p}{\partial y} = \rho g \frac{\partial \eta}{\partial y}. \tag{13.42}$$

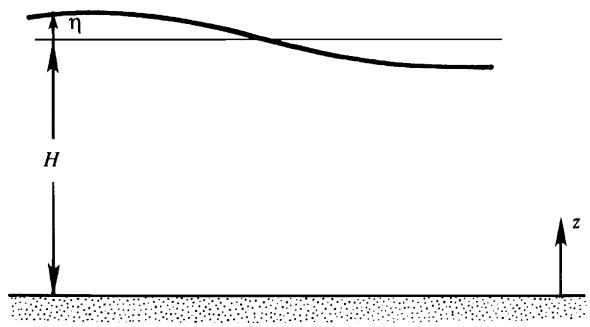

FIGURE 13.11 Geometry for a fluid layer of average thickness H above a flat bottom coincident with $z = 0$. At any horizontal location the liquid's surface height is $H + \eta$.

Since these are independent of z, the resulting horizontal motion is also depth independent so $\partial u/\partial x$ and $\partial v/\partial y$ are independent of z. Therefore, the continuity equation, $\partial u/\partial x + \partial v/\partial y + \partial w/\partial z = 0$, requires that w vary linearly with z, from zero at the bottom to the maximum value at the free surface. Integrating the continuity equation vertically across the water column from $z = 0$ to $z = H + \eta$, and noting that u and v are depth independent, we obtain

$$(H+\eta)\frac{\partial u}{\partial x} + (H+\eta)\frac{\partial v}{\partial y} + w(\eta) - w(0) = 0, \tag{13.43}$$

where $w(\eta)$ is the vertical velocity at the surface and $w(0) = 0$ is the vertical velocity at the bottom. The surface velocity is given by

$$w(\eta) = \frac{D\eta}{Dt} = \frac{\partial \eta}{\partial t} + u\frac{\partial \eta}{\partial x} + v\frac{\partial \eta}{\partial y},$$

which we recognize as the exact kinematic boundary condition on a free surface with two independent horizontal dimensions (*cf.* (7.17)). The continuity equation (13.43) then becomes

$$(H+\eta)\frac{\partial u}{\partial x} + (H+\eta)\frac{\partial v}{\partial y} + \frac{\partial \eta}{\partial t} + u\frac{\partial \eta}{\partial x} + v\frac{\partial \eta}{\partial y} = 0,$$

which can be written as

$$\frac{\partial \eta}{\partial t} + \frac{\partial}{\partial x}\Big[u(H+\eta)\Big] + \frac{\partial}{\partial y}\Big[v(H+\eta)\Big] = 0. \tag{13.44}$$

This says simply that the divergence of the horizontal fluid transport depresses the free surface. For small amplitude waves, the quadratic nonlinear terms can be neglected in comparison to the linear terms, so that the divergence term in (13.44) simplifies to $H\nabla\cdot\mathbf{u}$.

The linearized continuity and momentum equations are then:

$$\frac{\partial \eta}{\partial t} + H\left(\frac{\partial u}{\partial x} + \frac{\partial v}{\partial y}\right) = 0, \quad \frac{\partial u}{\partial t} - fv = -g\frac{\partial \eta}{\partial x}, \text{ and } \frac{\partial v}{\partial t} + fu = -g\frac{\partial \eta}{\partial y}. \tag{13.45}$$

In the momentum equations of (13.45), the pressure gradient terms are written in the form (13.42) and the nonlinear advective terms have been neglected under the small amplitude assumption. Equations (13.45), called the *shallow water equations*, govern the motion of a layer of fluid in which the horizontal scale is much larger than the depth of the layer. These equations will be used in the following sections for studying various types of gravity waves.

Although the preceding analysis has been formulated for a layer of *homogeneous* fluid, (13.45) are applicable to internal waves in a stratified medium, if we replace H by the *equivalent depth* H_e, defined by

$$c^2 = gH_e, \tag{13.46}$$

where c is the speed of long nonrotating *internal* gravity waves. This will be demonstrated in the following section.

13.9. NORMAL MODES IN A CONTINUOUSLY STRATIFIED LAYER

In the preceding section we considered a homogeneous medium and derived the governing equations for waves of wavelength larger than the depth of the fluid layer. Now consider a continuously stratified medium and assume that the horizontal scale of motion is much larger than the vertical scale. The pressure distribution is therefore hydrostatic, and the linearized equations of motion are:

$$\frac{\partial u}{\partial x}+\frac{\partial v}{\partial y}+\frac{\partial w}{\partial z}=0, \tag{13.47}$$

$$\frac{\partial u}{\partial t}-fv=-\frac{1}{\rho_0}\frac{\partial p}{\partial x},\ \frac{\partial v}{\partial t}+fu=-\frac{1}{\rho_0}\frac{\partial p}{\partial y}, \tag{13.48, 13.49}$$

$$0=-\frac{\partial p}{\partial z}-g\rho,\ \frac{\partial \rho}{\partial t}-\frac{\rho_0 N^2}{g}w=0, \tag{13.50, 13.51}$$

where p and ρ represent *perturbations* of pressure and density from the state of rest. The advective term in the density equation (13.51) is written in the linearized form $w(d\overline{\rho}/dz) = -\rho_0 N^2 w/g$, where $N(z)$ is the buoyancy frequency. In this form the rate of change of density at a point is assumed to be due only to the vertical advection of the background density distribution $\overline{\rho}(z)$, as discussed in Section 7.8.

In a continuously stratified medium, it is convenient to use the method of separation of variables and write $q = \sum q_n(x,y,t)\psi_n(z)$ for a dependent-field variable q. The solution is thus written as the sum of various vertical modes $\psi_n(z)$, which are called *normal modes* because they turn out to be orthogonal to each other. The vertical structure of a mode is described by ψ_n while q_n describes the horizontal propagation of the mode. Although each mode propagates only horizontally, the *sum* of a number of modes can also propagate vertically if the various q_n are out of phase.

We assume separable solutions of the form:

$$[u,v,p/\rho_0]=\sum_{n=0}^{\infty}[u_n,v_n,p_n]\psi_n(z), \tag{13.52}$$

$$w=\sum_{n=0}^{\infty}w_n\int_{-H}^{z}\psi_n(z)\,dz, \tag{13.53}$$

$$\rho=\sum_{n=0}^{\infty}\rho_n\frac{d\psi_n}{dz}, \tag{13.54}$$

where the amplitudes u_n, v_n, p_n, w_n, and ρ_n are functions of (x,y,t). The z-axis is measured from the upper free surface of the fluid layer, and $z=-H$ represents the bottom wall. The reasons for assuming the various forms of z-dependence in (13.52) through (13.54) are the following: Variables u, v, and p have the same vertical structure in order to be consistent with (13.48) and (13.49). The continuity equation (13.47) requires that the vertical structure of w should be the integral of $\psi_n(z)$. Equation (13.50) requires that the vertical structure of ρ must be the z-derivative of the vertical structure of p.

Substitution of (13.53) and (13.54) into (13.51) gives

$$\sum_{n=0}^{\infty}\left[\frac{\partial\rho_n}{\partial t}\frac{d\psi_n}{dz}-\frac{\rho_0 N^2}{g}w_n\int_{-H}^{z}\psi_n\,dz\right]=0.$$

This is valid for all values of z, and the modes are linearly independent, so the quantity within brackets must vanish for each mode, which implies

$$\frac{d\psi_n/dz}{N^2\int_{-H}^{z}\psi_n\,dz}=\frac{\rho_0}{g}\frac{w_n}{\partial\rho_n/\partial t}\equiv-\frac{1}{c_n^2}. \tag{13.55}$$

As the first term is a function of z alone and the second term is a function of (x,y,t) alone, for consistency both terms must be equal to a constant that we take to be $-1/c_n^2$. The vertical structure is then given by

$$\frac{1}{N^2}\frac{d\psi_n}{dz}=-\frac{1}{c_n^2}\int_{-H}^{z}\psi_n\,dz.$$

Taking the z-derivative,

$$\frac{d}{dz}\left(\frac{1}{N^2}\frac{d\psi_n}{dz}\right)+\frac{1}{c_n^2}\psi_n=0, \tag{13.56}$$

which is the differential equation governing the vertical structure of the normal modes. Equation (13.56) has the so-called Sturm-Liouville form, for which the various solutions are orthogonal.

Equation (13.55) also gives

$$w_n=-\frac{g}{\rho_0 c_n^2}\frac{\partial\rho_n}{\partial t}.$$

Substitution of (13.52) through (13.54) into (13.47) through (13.51) finally gives the normal mode equations:

$$\frac{\partial u_n}{\partial x}+\frac{\partial v_n}{\partial y}+\frac{1}{c_n^2}\frac{\partial p_n}{\partial t}=0, \tag{13.57}$$

$$\frac{\partial u_n}{\partial t}-fv_n=-\frac{\partial p_n}{\partial x},\quad \frac{\partial v_n}{\partial t}+fu_n=-\frac{\partial p_n}{\partial y}, \tag{13.58, 13.59}$$

$$p_n=-\frac{g}{\rho_0}\rho_n,\quad w_n=\frac{1}{c_n^2}\frac{\partial p_n}{\partial t}. \tag{13.60, 13.61}$$

Once (13.57) through (13.59) have been solved for u_n, v_n, and p_n, the amplitudes ρ_n and w_n can be obtained from (13.60) and (13.61). The set (13.57) through (13.59) is identical to the set (13.45) governing the motion of a *homogeneous* layer, provided p_n is identified with $g\eta$ and c_n^2 is identified with gH. In a stratified flow each mode (having a fixed vertical structure) behaves, in the horizontal dimensions and in time, just like a homogeneous layer, with an *equivalent depth* H_e defined by

$$c_n^2\equiv gH_e. \tag{13.62}$$

Boundary Conditions on ψ_n

At the bottom of the fluid layer, the boundary condition is

$$w = 0 \quad \text{at } z = -H.$$

To write this condition in terms of ψ_n, we first combine the hydrostatic equation (13.50) and the density equation (13.51) to give w in terms of p:

$$w = \frac{g(\partial\rho/\partial t)}{\rho_0 N^2} = -\frac{1}{\rho_0 N^2}\frac{\partial^2 p}{\partial z\,\partial t} = -\frac{1}{N^2}\sum_{n=0}^{\infty}\frac{\partial p_n}{\partial t}\frac{d\psi_n}{dz}. \tag{13.63}$$

The requirement $w = 0$ then yields the bottom boundary condition:

$$\frac{d\psi_n}{dz} = 0 \quad \text{at } z = -H. \tag{13.64}$$

We now formulate the surface boundary condition. The linearized surface boundary conditions are:

$$w = \frac{\partial\eta}{\partial t}, \quad p = \rho_0 g\eta \quad \text{at } z = 0, \tag{13.65′}$$

where η is the free surface displacement. These conditions can be combined into:

$$\frac{\partial p}{\partial t} = \rho_0 g w \quad \text{at } z = 0.$$

Using (13.63) this becomes:

$$\frac{g}{N^2}\frac{\partial^2 p}{\partial z\,\partial t} + \frac{\partial p}{\partial t} = 0 \quad \text{at } z = 0.$$

Substitution of the normal mode decomposition (13.52) gives:

$$\frac{d\psi_n}{dz} + \frac{N^2}{g}\psi_n = 0 \quad \text{at } z = 0. \tag{13.65}$$

The boundary conditions on ψ_n are therefore (13.64) and (13.65).

Vertical Mode Solution for Uniform N

For a medium of uniform N, a simple solution can be found for ψ_n. From (13.56), (13.64), and (13.65), the vertical structure of the normal modes is given by

$$\frac{d^2\psi_n}{dz^2} + \frac{N^2}{c_n^2}\psi_n = 0, \tag{13.66}$$

with the boundary conditions (13.64) and (13.65). The set (13.64) through (13.66) defines an eigenvalue problem, with ψ_n as the eigenfunction and c_n as the eigenvalue. The solution of (13.66) is

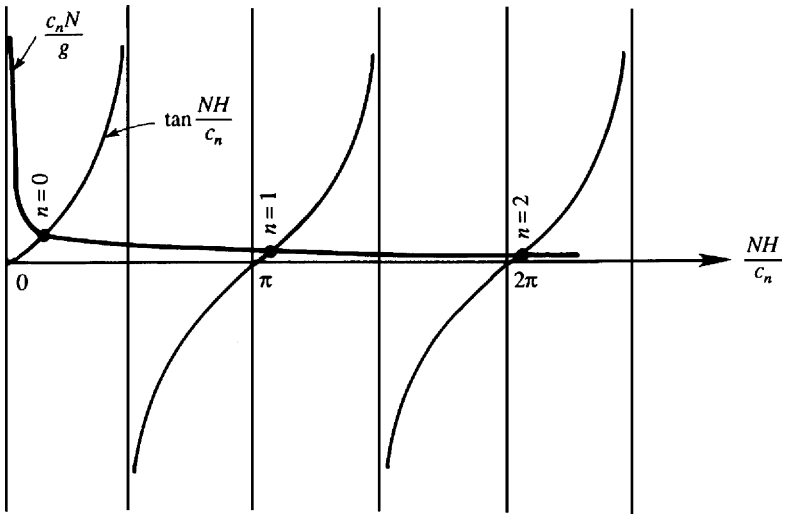

FIGURE 13.12 Calculation of eigenvalues c_n of vertical normal modes in a fluid layer of depth H and uniform stratification N. The eigenvalues occur where the curves defined by c_nN/g and $\tan(NH/c_n)$ cross. As drawn, these crossing points lie slightly above $n\pi$ for $n = 0$, 1, and 2.

$$\psi_n = A_n \cos\frac{Nz}{c_n} + B_n \sin\frac{Nz}{c_n}. \tag{13.67}$$

Application of the surface boundary condition (13.65) gives

$$B_n = -\frac{c_nN}{g}A_n. \tag{13.68}$$

The bottom boundary condition (13.64) then gives

$$\tan\frac{NH}{c_n} = \frac{c_nN}{g}, \tag{13.69}$$

whose roots define the eigenvalues of the problem.

The solution of (13.69) is indicated graphically in Figure 13.12. The first root occurs for $NH/c_n = 1$, for which we can write $\tan(NH/c_n) \approx NH/c_n$, so that (13.69) gives (indicating this root by $n = 0$):

$$c_0 = \sqrt{gH}. \tag{13.70}$$

The vertical modal structure is found from (13.67). Because the magnitude of an eigenfunction is arbitrary, we can set $A_0 = 1$, obtaining

$$\psi_0 = \cos\frac{Nz}{c_0} - \frac{c_0N}{g}\sin\frac{Nz}{c_0} \simeq 1 - \frac{N^2z}{g} \simeq 1,$$

where we have used $N|z|/c_0 \ll 1$ (with $NH/c_0 \ll 1$), and $N^2z/g \ll 1$ (with $N^2H/g = (NH/c_0)(c_0N/g) \ll 1$, both sides of (13.69) being much less than 1). For this mode the vertical structure of u, v, and p is therefore nearly depth independent. The corresponding structure for w (given by $\int \psi_0\, dz$, as indicated in (13.53)) is linear in z, with zero at the bottom and a maximum at the upper free surface. A stratified medium therefore has a mode of motion that behaves like that in an unstratified medium; this mode does not feel the stratification. The $n = 0$ mode is called the *barotropic mode*.

The remaining modes $n \geq 1$ are *baroclinic*. For these modes $c_nN/g \ll 1$ but NH/c_n is not small, as can be seen in Figure 13.12, so that the baroclinic roots of (13.69) are nearly given by

$$\tan\frac{NH}{c_n} = 0,$$

which gives

$$c_n = \frac{NH}{n\pi}, \qquad n = 1,2,3, \ldots. \tag{13.71}$$

Taking a typical depth-average oceanic value of $N \sim 10^{-3}$ s^{-1} and $H \sim 5$ km, the eigenvalue for the first baroclinic mode is $c_1 \sim 2$ m/s. The corresponding equivalent depth is $H_e = c_1^2/g \sim 0.4$ m.

An examination of the algebraic steps leading to (13.69) shows that neglecting the right-hand side is equivalent to replacing the upper boundary condition (13.65) by $w = 0$ at $z = 0$. This is called the *rigid lid approximation*. The *baroclinic modes are negligibly distorted by the rigid lid approximation*. In contrast, the rigid lid approximation applied to the *barotropic* mode would yield $c_0 = \infty$, as (13.71) shows for $n = 0$. Note that the rigid lid approximation does *not* imply that the free surface displacement corresponding to the baroclinic modes is negligible in the ocean. In fact, excluding the wind waves and tides, much of the free surface displacements in the ocean are due to baroclinic motions. The rigid lid approximation merely implies that, for baroclinic motions, the vertical displacements at the surface are much smaller than those within the fluid column. A valid baroclinic solution can therefore be obtained by setting $w = 0$ at $z = 0$. Further, the rigid lid approximation does not imply that the pressure is constant at the level surface $z = 0$; if a rigid lid were actually imposed at $z = 0$, then the pressure on the lid would vary due to the baroclinic motions.

The vertical mode shape under the rigid lid approximation is given by the cosine distribution

$$\psi_n = \cos\frac{n\pi z}{H}, \quad n = 0,1,2,\ldots,$$

because it satisfies $d\psi_n/dz = 0$ at $z = 0, -H$. The nth mode ψ_n has n zero crossings within the layer (Figure 13.13).

A decomposition into normal modes is only possible in the absence of topographic variations and mean currents with shear. It is valid with or without Coriolis forces and with or without the β-effect. However, the hydrostatic approximation here means that the frequencies are much smaller than N. Under this condition the eigenfunctions are independent of the frequency, as (13.56) shows. Without the hydrostatic approximation the eigenfunctions ψ_n become dependent on the frequency ω. This is discussed, for example, in LeBlond and Mysak (1978).

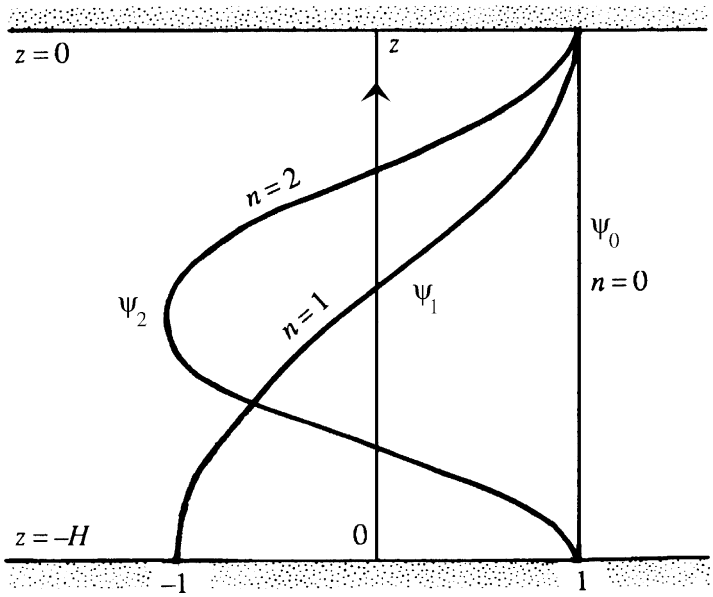

FIGURE 13.13 Vertical distributions of the first three normal modes in a stratified medium of uniform buoyancy frequency for a fluid layer of depth H. The first mode ($n = 0$) is nearly uniform through the depth. The second mode ($n = 1$) shows one-half wavelength in $-H < z < 0$. The third mode ($n = 2$) shows one full wavelength in $-H < z < 0$. Note that all modes must have $d\psi_n/dz = 0$ on $z = -H$, while $d\psi_n/dz$ is only approximately zero a $z = 0$.

Summary

Small amplitude motion in a frictionless continuously stratified ocean can be decomposed in terms of noninteracting vertical normal modes. The vertical structure of each mode is defined by an eigenfunction $\psi_n(z)$. If the horizontal scale of the waves is much larger than the vertical scale, then the equations governing the horizontal propagation of each mode are identical to those of a shallow *homogeneous* layer, with the layer depth H replaced by an equivalent depth H_e defined by $c_n^2 = gH_e$. For a medium of constant N, the baroclinic ($n \geq 1$) eigenvalues are given by $c_n = NH/\pi n$, while the barotropic eigenvalue is $c_0 = \sqrt{gH}$. The rigid lid approximation is quite good for the baroclinic modes.

13.10. HIGH- AND LOW-FREQUENCY REGIMES IN SHALLOW-WATER EQUATIONS

We shall now examine what terms are negligible in the shallow-water equations for the various frequency ranges. Our analysis is valid for a single homogeneous layer or for a stratified medium. In the latter case H has to be interpreted as the *equivalent* depth, and c has to be interpreted as the speed of long nonrotating *internal* gravity waves. The β-effect is considered in this section. As f varies only northward, horizontal isotropy is lost whenever the β-effect is included, and it becomes necessary to distinguish between the different horizontal directions. We shall follow the usual geophysical convention that the x-axis is directed eastward and the y-axis is directed northward, with u and v the corresponding velocity components.

The simplest way to perform the analysis is to examine the v-equation. A single equation for v can be derived by first taking the time derivatives of the momentum equations in (13.45) and using the continuity equation to eliminate $\partial\eta/\partial t$. This gives

$$\frac{\partial^2 u}{\partial t^2} - f\frac{\partial v}{\partial t} = gH\frac{\partial}{\partial x}\left(\frac{\partial u}{\partial x} + \frac{\partial v}{\partial y}\right), \quad \frac{\partial^2 v}{\partial t^2} + f\frac{\partial u}{\partial t} = gH\frac{\partial}{\partial y}\left(\frac{\partial u}{\partial x} + \frac{\partial v}{\partial y}\right). \tag{13.72, 13.73}$$

Now take $\partial/\partial t$ of (13.73) and use (13.72) to obtain

$$\frac{\partial^3 v}{\partial t^3} + f\left[f\frac{\partial v}{\partial t} + gH\frac{\partial}{\partial x}\left(\frac{\partial u}{\partial x} + \frac{\partial v}{\partial y}\right)\right] = gH\frac{\partial^2}{\partial y\,\partial t}\left(\frac{\partial u}{\partial x} + \frac{\partial v}{\partial y}\right). \tag{13.74}$$

To eliminate u, we first obtain a vorticity equation by cross differentiating and subtracting the momentum equations in (13.45):

$$\frac{\partial}{\partial t}\left(\frac{\partial u}{\partial y} - \frac{\partial v}{\partial x}\right) - f_0\left(\frac{\partial u}{\partial x} + \frac{\partial v}{\partial y}\right) - \beta v = 0.$$

Here, we have made the customary β-plane approximation valid if the y-scale is small enough so that $\Delta f/f \ll 1$. Accordingly, we have treated f as constant (and replaced it by an average value f_0) *except* when df/dy appears; this is why we have written f_0 in the second term of the preceding equation. Taking the x-derivative, multiplying by gH, and adding to (13.74), we finally obtain a vorticity equation in terms of v only:

$$\frac{\partial^3 v}{\partial t^3} - gH\frac{\partial}{\partial t}\nabla_{\mathrm{H}}^2 v + f_0^2\frac{\partial v}{\partial t} - gH\beta\frac{\partial v}{\partial x} = 0, \tag{13.75}$$

where $\nabla_{\mathrm{H}}^2 = \partial^2/\partial x^2 + \partial^2/\partial y^2$ is the horizontal Laplacian operator.

Equation (13.75) is Boussinesq, linear, and hydrostatic, but otherwise quite general in the sense that it is applicable to both high and low frequencies. Consider wave solutions of the form

$$v = \hat{v}\, e^{i(kx+ly-\omega t)},$$

where k is the eastward wave number and l is the northward wave number. Then (13.75) gives

$$\omega^3 - c^2\omega K^2 - f_0^2\omega - c^2\beta k = 0, \tag{13.76}$$

where $K^2 = k^2 + l^2$ and $c = \sqrt{gH}$. It can be shown that all roots of (13.76) are real, two of the roots being superinertial ($\omega \gg f$) and the third being subinertial ($\omega \ll f$). Equation (13.76) is the complete dispersion relation for linear shallow-water equations. In various parametric ranges it takes simpler forms, representing simpler waves.

First, consider high-frequency waves $\omega \gg f$. The third term of (13.76) is negligible compared to the first term. Moreover, the fourth term is also negligible in this range. Compare, for example, the fourth and second terms:

$$\frac{c^2\beta k}{c^2\omega K^2} \sim \frac{\beta}{\omega K} \sim 10^{-3},$$

where we have assumed typical values of $\beta = 2 \times 10^{-11}$ m^{-1} s^{-1}, $\omega = 3f \sim 3 \times 10^{-4}$ s^{-1}, and $2\pi/K \sim 100$ km. For $\omega \gg f$, therefore, the balance is between the first and second terms in (13.76), and the roots are $\omega = \pm K\sqrt{gH}$, which correspond to a propagation speed of $\omega/K = \sqrt{gH}$. The effects of both f and β are therefore negligible for high-frequency waves, as is expected as they are too fast to be affected by the Coriolis effects.

Next consider $\omega > f$, but $\omega \sim f$. Then the third term in (13.76) is not negligible, but the β-effect is. These are gravity waves influenced by Coriolis forces; gravity waves are discussed in the next section. However, the time scales are still too short for the motion to be affected by the β-effect.

Last, consider very slow waves for which $\omega \ll f$. Then the β-effect becomes important, and the first term in (13.76) becomes negligible. Compare, for example, the first and the last terms:

$$\frac{\omega^3}{c^2 \beta k} \ll 1.$$

Typical values for the ocean are $c \sim 200$ m/s for the barotropic mode, $c \sim 2$ m/s for the baroclinic mode, $\beta = 2 \times 10^{-11}$ m^{-1} s^{-1}, $2\pi/k \sim 100$ km, and $\omega \sim 10^{-5}$ s^{-1}. This makes the aforementioned ratio about 0.2×10^{-4} for the barotropic mode and 0.2 for the baroclinic mode. The first term in (13.76) is therefore negligible for $\omega \gg f$.

Equation (13.75) governs the dynamics of a variety of wave motions in the ocean and the atmosphere, and the discussion in this section shows what terms can be dropped under various limiting conditions. An understanding of these limiting conditions will be useful in the following sections.

13.11. GRAVITY WAVES WITH ROTATION

In this chapter we examine several free-wave solutions of the shallow-water equations. In this section we focus on gravity waves with frequencies in the range $\omega > f$, for which the β-effect is negligible, as demonstrated in the preceding section. Consequently, the Coriolis frequency f is regarded as constant here. Consider progressive waves of the form

$$(u, v, \eta) = (\hat{u}, \hat{v}, \hat{\eta}) e^{i(kx+ly-\omega t)},$$

where $\hat{u}$, $\hat{v}$, and $\hat{\eta}$ are the complex amplitudes, and the real part of the right-hand side is meant. Then (13.45) gives

$$-i\omega\hat{u} - f\hat{v} = -ikg\hat{\eta}, \; -i\omega\hat{v} + f\hat{u} = -ilg\hat{\eta}, \; -i\omega\hat{\eta} + iH(k\hat{u} + l\hat{v}) = 0. \quad (13.77, 13.78, 13.79)$$

Solving for $\hat{u}$ and $\hat{v}$ between (13.77) and (13.78), we obtain:

$$\begin{aligned} \hat{u} &= \frac{g\hat{\eta}}{\omega^2 - f^2}(\omega k + ifl), \\ \hat{v} &= \frac{g\hat{\eta}}{\omega^2 - f^2}(-ifk + \omega l). \end{aligned} \quad (13.80)$$

Substituting these in (13.79), we obtain

$$\omega^2 - f^2 = gH(k^2 + l^2). \tag{13.81}$$

This is the dispersion relation of gravity waves in the presence of Coriolis forces. (The relation can be most simply derived by setting the determinant of the set of linear homogeneous equations (13.77) through (13.79) to zero.) It can be written as

$$\omega^2 = f^2 + gHK^2, \tag{13.82}$$

where $K = \sqrt{k^2 + l^2}$ is the magnitude of the horizontal wave number. The dispersion relation shows that the waves can propagate in any horizontal direction and have $\omega > f$. Gravity waves affected by Coriolis forces are called *Poincaré waves*, *Sverdrup waves*, or simply *rotational gravity waves*. (Sometimes the name "Poincaré wave" is used to describe those rotational gravity waves that satisfy the boundary conditions in a channel.) In spite of its names, the solution was first worked out by Kelvin (Gill, 1982, p. 197). A plot of (13.82) is shown in Figure 13.14. It is seen that the waves are dispersive except for $\omega \gg f$ when equation (13.82) gives $\omega^2 \approx gHK^2$, so that the propagation speed is $\omega/K = \sqrt{gH}$. The high-frequency limit agrees with our previous discussion of surface gravity waves unaffected by Coriolis forces.

Particle Orbit

The symmetry of the dispersion relation (13.81) with respect to k and l means that the x- and y-directions are not felt differently by the wave field. The horizontal isotropy is a result of treating f as constant. (We shall see later that Rossby waves, which depend on the β-effect, are not horizontally isotropic.) We can therefore orient the x-axis along the wave number

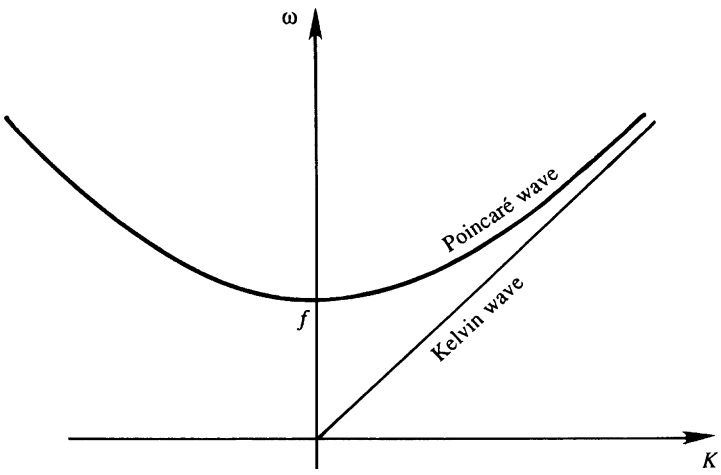

FIGURE 13.14 Dispersion relations for Poincaré and Kelvin waves. Here, ω is the wave frequency. K is the magnitude of the wave number, and f is the local inertial frequency. At frequencies $\omega \gg f$, the ordinary shallow-water wave dispersion relationship $\omega^2 = gHK^2$ is recovered.

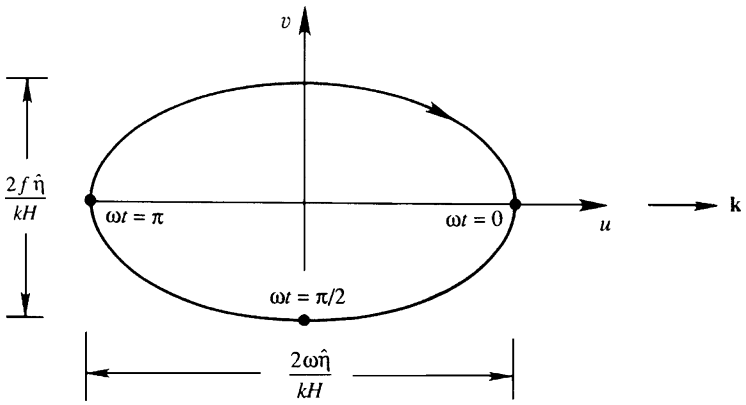

FIGURE 13.15 Particle orbit in a gravity wave traveling in the positive x-direction. Looking down on the surface, the orbit is an ellipse having major and minor axes proportional to the wave frequency ω and the inertial frequency f. Velocity components corresponding to $\omega t = 0$, $\pi/2$, and π are indicated.

vector and set $l = 0$, so that the wave field is invariant along the y-axis. To find the particle orbits, it is convenient to work with real quantities. Let the displacement be

$$\eta = \hat{\eta} \cos(kx - \omega t),$$

where $\hat{\eta}$ is real. The corresponding velocity components can be found by multiplying (13.80) by $\exp(ikx - i\omega t)$ and taking the real part of both sides. This gives

$$\begin{aligned} u &= \frac{\omega\hat{\eta}}{kH}\cos(kx - \omega t), \\ v &= \frac{f\hat{\eta}}{kH}\sin(kx - \omega t). \end{aligned} \tag{13.83}$$

To find the particle paths, take $x = 0$ and consider three values of time corresponding to $\omega t = 0$, $\pi/2$, and π. The corresponding values of u and v from (13.83) show that the velocity vector rotates clockwise (in the northern hemisphere) in elliptic paths (Figure 13.15). The ellipticity is expected, since the presence of Coriolis forces means that fu must generate $\partial v/\partial t$ according to the equation of motion (13.45). (In equation (13.45), $\partial\eta/\partial y = 0$ due to our orienting the x-axis along the direction of propagation of the wave.) Particles are therefore constantly deflected to the right by the Coriolis force, resulting in elliptic orbits. *The ellipses have an axis ratio of ω/f and the major axis is oriented in the direction of wave propagation*. The ellipses become narrower as ω/f increases, approaching the rectilinear orbit of gravity waves unaffected by planetary rotation. However, the sea surface in a rotational gravity wave is no different from that for ordinary gravity waves, namely oscillatory in the direction of propagation and invariant in the perpendicular direction.

Inertial Motion

Consider the limit $\omega \to f$, that is, when the particle paths are circular. The dispersion relation (13.82) then shows that $K \to 0$, implying a horizontal uniformity of the flow field. Equation (13.79) shows that $\hat{\eta}$ must tend to zero in this limit, so that there are no horizontal

pressure gradients in this limit. Because $\partial u/\partial x = \partial v/\partial y = 0$, the continuity equation shows that $w = 0$. The particles therefore move on horizontal sheets, each layer decoupled from the one above and below it. The balance of forces is

$$\partial u/\partial t - fv = 0 \quad \text{and} \quad \partial v/\partial t + fu = 0.$$

The solution of this set is of the form

$$u = q\cos(ft) \quad \text{and} \quad v = -q\sin(ft),$$

where the speed $q = \sqrt{u^2 + v^2}$ is constant along the path. The radius r of the orbit can be found by adopting a Lagrangian point of view, and noting that the equilibrium of forces is between the Coriolis acceleration fq and the centrifugal acceleration $r\omega^2 = rf^2$, giving $r = q/f$. The limiting case of motion in circular orbits at a frequency f is called *inertial motion*, because in the absence of pressure gradients a particle moves by virtue of its inertia alone. The corresponding period $2\pi/f$ is called the *inertial period*. In the absence of planetary rotation such motion would be along straight lines; in the presence of Coriolis forces the motion is along circular paths, called *inertial circles*. Near-inertial motion is frequently generated in the surface layer of the ocean by sudden changes of the wind field, essentially because the equations of motion (13.45) have a natural frequency f. Taking a typical current magnitude of $q \sim 0.1$ m/s, the radius of the orbit is $r \sim 1$ km.

13.12. KELVIN WAVE

In the preceding section we considered a shallow-water gravity wave propagating in a horizontally *unbounded* ocean. We saw that the crests are horizontal and oriented in a direction perpendicular to the direction of propagation. The *absence* of a transverse pressure gradient $\partial\eta/\partial y$ resulted in a transverse flow and elliptic orbits. This is clear from the third equation in (13.45), which shows that the presence of fu must result in $\partial v/\partial t$ if $\partial\eta/\partial y = 0$. In this section we consider a gravity wave propagating parallel to a wall, whose presence allows a pressure gradient $\partial\eta/\partial y$ that can decay away from the wall. We shall see that this allows a gravity wave in which fu is geostrophically balanced by $-g(\partial\eta/\partial y)$, and $v = 0$. Consequently the particle orbits are not elliptic but rectilinear.

Consider first a gravity wave propagating in a channel. From Figure 7.5 we know that the fluid velocity under a crest is in the direction of wave propagation, and that under a trough it is the opposite. Figure 13.16 shows two transverse sections of the wave, one through a crest (left panel) and the other through a trough (right panel). The wave is propagating into the plane of the paper, along the x-direction. Then the fluid velocity under the crest is into the plane of the paper and that under the trough is out of the plane of the paper. The constraints of the sidewalls require that $v = 0$ at the walls, and we are exploring the possibility of a wave motion in which v is zero everywhere. Then the equation of motion along the y-direction requires that fu can only be geostrophically balanced by a transverse slope of the sea surface across the channel:

$$fu = -g\frac{\partial\eta}{\partial y}.$$

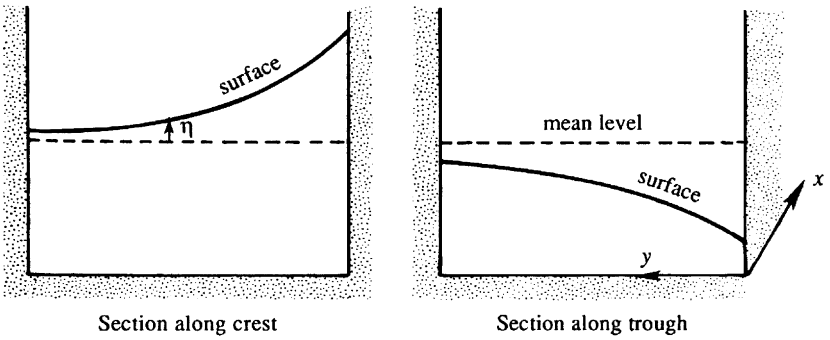

FIGURE 13.16 Free surface distribution in a Kelvin gravity wave propagating into the plane of the paper (the x-direction) within a channel. The wave crests and troughs are enhanced on the right side of the channel.

In the northern hemisphere, the surface must slope as indicated in the figure, that is, downward to the left under the crest and upward to the left under the trough, so that the pressure force has the current directed to its right. The result is that the amplitude of the wave is larger on the right-hand side of the channel, looking into the direction of propagation, as indicated in Figure 13.16. The current amplitude, like the surface displacement, also decays to the left.

If the left wall in Figure 13.16 is moved away to infinity, we get a gravity wave trapped to the coast (Figure 13.17). A coastally trapped long gravity wave, in which the transverse velocity $v = 0$ everywhere, is called a *Kelvin wave*. It is clear that it can propagate only in a direction such that the coast is to the right (looking in the direction of propagation) in the northern hemisphere and to the left in the southern hemisphere. The opposite direction of propagation would result in a sea surface displacement increasing exponentially away from the coast, which is not possible.

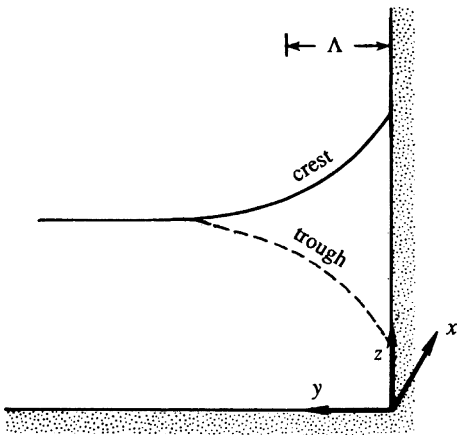

FIGURE 13.17 Coastal Kelvin wave propagating along the x-axis. The sea surface shape across a section through a crest is indicated by the continuous line, and that along a trough is indicated by the dashed line.

An examination of the transverse momentum equation,

$$\frac{\partial v}{\partial t} + fu = -g\frac{\partial \eta}{\partial y},$$

reveals fundamental differences between Poincaré waves and Kelvin waves. For a Poincaré wave the crests are horizontal, and the absence of a transverse pressure gradient requires a $\partial v/\partial t$ to balance the Coriolis force, resulting in elliptic orbits. In a Kelvin wave a transverse velocity is prevented by a geostrophic balance of fu and $-g(\partial\eta/\partial y)$.

From the shallow-water set (13.45), the equations of motion for a Kelvin wave propagating along a coast aligned with the x-axis (Figure 13.17) are:

$$\frac{\partial \eta}{\partial t} + H\frac{\partial u}{\partial x} = 0,\ \frac{\partial u}{\partial t} = -g\frac{\partial \eta}{\partial x},\ \text{and}\ fu = -g\frac{\partial \eta}{\partial y}. \tag{13.84}$$

Assume a solution of the form:

$$[u, \eta] = \left[\widehat{u}(y), \widehat{\eta}(y)\right] e^{i(kx-\omega t)}.$$

Then (13.84) gives

$$\begin{aligned} -i\omega\widehat{\eta} + iHk\widehat{u} &= 0, \\ -i\omega\widehat{u} &= -igk\widehat{\eta}, \\ f\widehat{u} &= -g\frac{d\widehat{\eta}}{dy}. \end{aligned} \tag{13.85}$$

The dispersion relation can be found solely from the first two of these equations; the third equation then determines the transverse structure. Eliminating $\hat{u}$ between the first two, we obtain

$$\widehat{\eta}\left[\omega^2 - gHk^2\right] = 0.$$

A nontrivial solution is therefore possible only if $\omega = \pm k\sqrt{gH}$, so that the wave propagates with a nondispersive speed:

$$c = \sqrt{gH}. \tag{13.86}$$

The propagation speed of a Kelvin wave is therefore identical to that of nonrotating gravity waves. Its dispersion equation is a straight line and is shown in Figure 13.14. All frequencies are possible.

To determine the transverse structure, eliminate $\widehat{u}$ between the first and third equation of (13.85), giving

$$\frac{d\widehat{\eta}}{dy} \pm \frac{f}{c}\widehat{\eta} = 0.$$

The solution that decays away from the coast is

$$\widehat{\eta} = \eta_0\, e^{-fy/c},$$

where η_0 is the amplitude at the coast. Therefore, the sea surface slope and the velocity field for a Kelvin wave have the form:

$$\begin{aligned} \eta &= \eta_0 e^{-fy/c} \cos k(x - ct), \\ u &= \eta_0 \sqrt{\frac{g}{H}} e^{-fy/c} \cos k(x - ct), \end{aligned} \tag{13.87}$$

where we have taken the real parts, and have used equation (13.85) in obtaining the u field.

Equations (13.87) show that the transverse decay scale of the Kelvin wave is

$$\Lambda \equiv \frac{c}{f},$$

which is called the *Rossby radius of deformation*. For a deep sea of depth $H = 5$ km, and a mid-latitude value of $f = 10^{-4}$ s^{-1}, we obtain $c = \sqrt{gH} = 220$ m/s and $\Lambda = c/f = 2200$ km. Tides are frequently in the form of coastal Kelvin waves of semidiurnal frequency. The tides are forced by the periodic changes in the gravitational attraction of the moon and the sun. These waves propagate along the boundaries of an ocean basin and cause sea level fluctuations at coastal stations.

Analogous to the surface or "external" Kelvin waves discussed in the preceding paragraphs, we can have *internal Kelvin waves* at the interface between two fluids of different densities (Figure 13.18). If the lower layer is very deep, then the speed of propagation is given by (see (7.117)):

$$c = \sqrt{g'H},$$

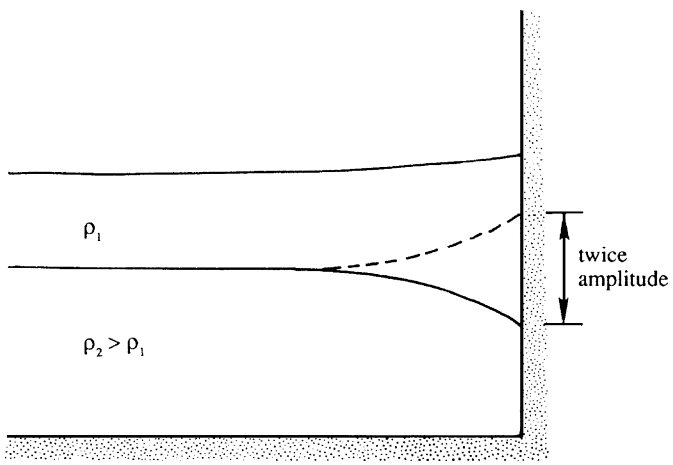

FIGURE 13.18 Internal Kelvin wave at an interface. Dashed line indicates position of the interface when it is at its maximum height. Displacement of the free surface is much smaller than that of the interface and is oppositely directed.

where H is the thickness of the upper layer and $g' = g(\rho_2 - \rho_1)/\rho_2$ is the reduced gravity. For a continuously stratified medium of depth H and buoyancy frequency N internal Kelvin waves can propagate at any of the normal mode speeds

$$c = NH/n\pi, \qquad n = 1,2,\ldots.$$

The decay scale for *internal* Kelvin waves, $\Lambda = c/f$, is called the *internal Rossby radius of deformation*, whose value is much smaller than that for the external Rossby radius of deformation. For $n = 1$, a typical value in the ocean is $\Lambda = NH/\pi f \sim 50$ km; a typical atmospheric value is much larger, being of order $\Lambda \sim 1000$ km.

Internal Kelvin waves in the ocean are frequently forced by wind changes near coastal areas. For example, a southward wind along the west coast of a continent in the northern hemisphere (say, California) generates an Ekman layer at the ocean surface, in which the mass flow is *away* from the coast (to the right of the applied wind stress). The mass flux in the near-surface layer is compensated by the movement of deeper water toward the coast, which raises the thermocline. An upward movement of the thermocline, as indicated by the dashed line in Figure 13.18, is called *upwelling*. The vertical movement of the thermocline in the wind-forced region then propagates poleward along the coast as an internal Kelvin wave.

13.13. POTENTIAL VORTICITY CONSERVATION IN SHALLOW-WATER THEORY

In this section we shall derive a useful conservation law for the vorticity of a shallow layer of fluid. From Section 13.8, the equations of motion for a shallow layer of homogeneous fluid are:

$$\frac{\partial u}{\partial t} + u\frac{\partial u}{\partial x} + v\frac{\partial u}{\partial y} - fv = -g\frac{\partial \eta}{\partial x}, \tag{13.88}$$

$$\frac{\partial v}{\partial t} + u\frac{\partial v}{\partial x} + v\frac{\partial v}{\partial y} + fu = -g\frac{\partial \eta}{\partial y}, \tag{13.89}$$

$$\frac{\partial h}{\partial t} + \frac{\partial}{\partial x}(uh) + \frac{\partial}{\partial y}(vh) = 0, \tag{13.90}$$

where $h(x,y,t)$ is the depth of flow and η is the height of the sea surface measured from an arbitrary horizontal plane (Figure 13.19). The x-axis is taken eastward and the y-axis is taken northward, with u and v the corresponding velocity components. The Coriolis frequency $f = f_0 + \beta y$ is regarded as dependent on latitude. The nonlinear terms have been retained, including those in the continuity equation, which has been written in the form (13.44); note that $h = H + \eta$. We saw in Section 13.8 that the constant density of the layer and the hydrostatic pressure distribution make the horizontal pressure gradient depth independent, so that only a depth-independent current can be generated. The vertical velocity is linear in z.

A vorticity equation can be derived by differentiating (13.88) with respect to y, (13.89) with respect to x, and subtracting. As expected, these steps eliminate the pressure, and we obtain:

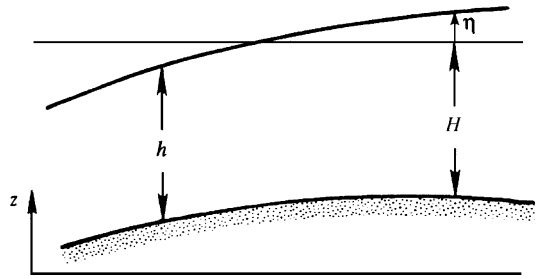

FIGURE 13.19 Shallow layer of instantaneous depth $h(x,y,t)$ when the ocean bottom is not flat. Here η is the sea surface deflection measured from a conveniently chosen horizontal plane.

$$\frac{\partial}{\partial t}\left(\frac{\partial v}{\partial x}-\frac{\partial u}{\partial y}\right)+\frac{\partial}{\partial x}\left[u\frac{\partial v}{\partial x}+v\frac{\partial v}{\partial y}\right]-\frac{\partial}{\partial y}\left[u\frac{\partial u}{\partial x}+v\frac{\partial u}{\partial y}\right]+f_0\left(\frac{\partial u}{\partial x}+\frac{\partial v}{\partial y}\right)+\beta v = 0. \tag{13.91}$$

Following the customary β-plane approximation, we have treated f as constant (and replaced it by an average value f_0) *except* when df/dy appears. We now introduce

$$\zeta \equiv \frac{\partial v}{\partial x}-\frac{\partial u}{\partial y}$$

as the vertical component of *relative vorticity*, that is, the vorticity measured relative to the rotating earth. Then the nonlinear terms in (13.91) can easily be rearranged in the form

$$u\frac{\partial \zeta}{\partial x}+v\frac{\partial \zeta}{\partial y}+\left(\frac{\partial u}{\partial x}+\frac{\partial v}{\partial y}\right)\zeta.$$

Equation (13.91) then becomes

$$\frac{\partial \zeta}{\partial t}+u\frac{\partial \zeta}{\partial x}+v\frac{\partial \zeta}{\partial y}+\left(\frac{\partial u}{\partial x}+\frac{\partial v}{\partial y}\right)(\zeta+f_0)+\beta v = 0,$$

which can be written as

$$\frac{D\zeta}{Dt}+(\zeta+f_0)\left(\frac{\partial u}{\partial x}+\frac{\partial v}{\partial y}\right)+\beta v = 0, \tag{13.92}$$

where D/Dt is the derivative following the horizontal motion of the layer:

$$\frac{D}{Dt}\equiv\frac{\partial}{\partial t}+u\frac{\partial}{\partial x}+v\frac{\partial}{\partial y}.$$

The horizontal divergence $(\partial u/\partial x+\partial v/\partial y)$ in (13.92) can be eliminated by using the continuity equation (13.90), which can be written as

$$\frac{Dh}{Dt}+h\left(\frac{\partial u}{\partial x}+\frac{\partial v}{\partial y}\right)=0.$$

Equation (13.92) then becomes

$$\frac{D\zeta}{Dt} = \frac{\zeta + f_0}{h}\frac{Dh}{Dt} - \beta v.$$

This can be written as

$$\frac{D(\zeta + f)}{Dt} = \frac{\zeta + f_0}{h}\frac{Dh}{Dt}, \tag{13.93}$$

where we have used

$$\frac{Df}{Dt} = \frac{\partial f}{\partial t} + u\frac{\partial f}{\partial x} + v\frac{\partial f}{\partial y} = v\beta.$$

Because of the absence of vertical shear, the vorticity in a shallow-water model is purely vertical and independent of depth. The relative vorticity measured with respect to the rotating earth is ζ, while f is the planetary vorticity, so that the *absolute vorticity* is $(\zeta + f)$. Equation (13.93) shows that the rate of change of absolute vorticity is proportional to the absolute vorticity times the vertical stretching Dh/Dt of the water column. It is apparent that $D\zeta/Dt$ can be nonzero even if $\zeta = 0$ initially. This is different from a nonrotating flow in which stretching a fluid line changes its vorticity only if the line has an *initial* vorticity. (This is why the process was called the *vortex* stretching; see Section 5.7.) The difference arises because vertical lines in a rotating earth contain the planetary vorticity even when $\zeta = 0$. Note that the vortex *tilting* term, discussed in Section 5.6, is absent in the shallow-water theory because the water moves in the form of vertical columns without ever tilting.

Equation (13.93) can be written in the compact form

$$\frac{D}{Dt}\left(\frac{\varsigma + f}{h}\right) = 0, \tag{13.94}$$

where $f = f_0 + \beta y$, and we have assumed $\beta y \ll f_0$. The ratio $(\zeta + f)/h$ is called the *potential vorticity* in shallow-water theory. Equation (13.94) shows that the *potential vorticity is conserved along the motion*, an important principle in geophysical fluid dynamics. In the ocean, outside regions of strong current vorticity such as coastal boundaries, the magnitude of ζ is much smaller than that of f. In such a case $(\zeta + f)$ has the sign of f. The principle of conservation of potential vorticity means that an increase in h must make $(\zeta + f)$ more positive in the northern hemisphere and more negative in the southern hemisphere.

As an example of application of the potential vorticity equation, consider an eastward flow over a step (at $x = 0$) running north–south, across which the layer thickness changes discontinuously from h_0 to h_1 (Figure 13.20). The flow upstream of the step has a uniform speed U, so that the oncoming stream has no relative vorticity. To conserve the ratio $(\zeta + f)/h$, the flow must suddenly acquire negative (clockwise) relative vorticity due to the sudden decrease in layer thickness. The relative vorticity of a fluid element just after passing the step can be found from

$$\frac{f}{h_0} = \frac{\zeta + f}{h_1},$$

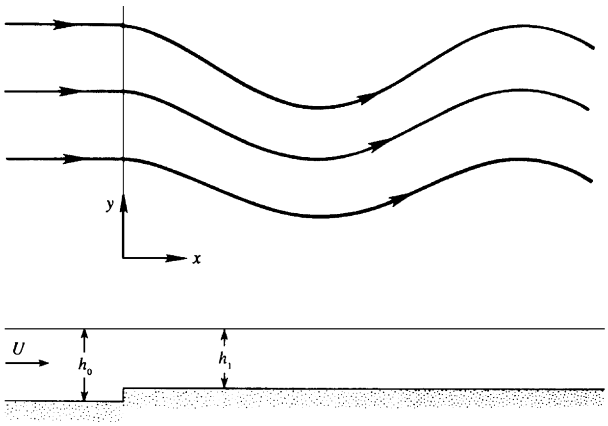

FIGURE 13.20 Eastward flow over a step change in depth. Looking down from above, the step causes southward deflection of the streamlines that is eventually countered by latitude change and results in stationary spatial oscillations of wavelength $2\pi\sqrt{U/\beta}$.

giving $\zeta = f(h_1 - h_0)/h_0 < 0$, where f is evaluated at the upstream latitude of the streamline. Because of the clockwise vorticity, the fluid starts to move south at $x = 0$. The southward movement decreases f, so that ζ must correspondingly increase to keep $(f + \zeta)$ constant. This means that the clockwise curvature of the stream reduces, and eventually becomes a counterclockwise curvature. In this manner an eastward flow over a step generates stationary undulatory flow on the downstream side. In Section 13.15 we shall see that the stationary oscillation is due to a Rossby wave generated at the step whose westward phase velocity is canceled by the eastward current. We shall see that the wavelength is $2\pi\sqrt{U/\beta}$.

Suppose we try the same argument for a *westward* flow over a step. Then a particle should suddenly acquire clockwise vorticity as the depth of flow decreases at $x = 0$, which

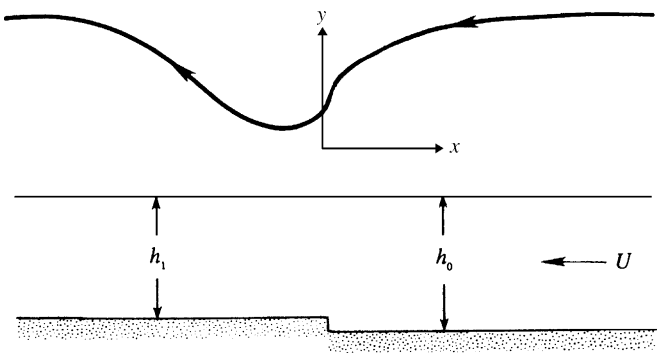

FIGURE 13.21 Westward flow over a step change in depth. Unlike the eastward flow depicted in Figure 13.20, the westward flow is not oscillatory and feels the upstream influence of the step. Looking down from above, the step causes one southward deflection that starts before the step and recovers after it.

would require the particle to move north. It would then come into a region of larger f, which would require ζ to decrease further. Clearly, an exponential behavior is predicted, suggesting that the argument is not correct. Unlike an eastward flow, a westward current feels the *upstream* influence of the step so that it acquires a counterclockwise curvature *before* it encounters the step (Figure 13.21). The positive vorticity is balanced by a reduction in f, which is consistent with conservation of potential vorticity. At the location of the step the vorticity decreases suddenly. Finally, far downstream of the step a fluid particle is again moving westward at its original latitude. The westward flow over a topography is *not* oscillatory.

13.14. INTERNAL WAVES

In Chapter 7.8 we studied internal gravity waves unaffected by Coriolis forces. We saw that they are not isotropic; in fact the direction of propagation with respect to the vertical determines their frequency. We also saw that their frequency satisfies the inequality $\omega \leq N$, where N is the buoyancy frequency. Their phase-velocity vector $\mathbf{c}$ and the group-velocity vector $\mathbf{c}_g$ are perpendicular and have oppositely directed vertical components (Figure 7.29 and Figure 7.31). That is, phases propagate upward if the groups propagate downward, and vice versa. In this section we shall study the effect of Coriolis forces on internal waves, assuming that f is independent of latitude.

Internal waves are ubiquitous in the atmosphere and the ocean. In the lower atmosphere turbulent motions dominate, so that internal wave activity represents a minor component of the motion. In contrast, the stratosphere contains a great deal of internal wave activity, and very little convective motion, because of its stable density distribution. They generally propagate upward from the lower atmosphere, where they are generated. In the ocean they may be as common as the waves on the surface, and measurements show that they can cause the isotherms to go up and down by as much as 50–100 m. Sometimes the internal waves break and generate smaller-scale turbulence in a somewhat similar manner to bubble and foam generation by breaking surface waves.

We shall now examine the nature of the fluid motion in internal waves. The equations of motion are:

$$\begin{aligned}
&\frac{\partial u}{\partial x}+\frac{\partial v}{\partial y}+\frac{\partial w}{\partial z}=0,\\
&\frac{\partial u}{\partial t}-fv=-\frac{1}{\rho_0}\frac{\partial p}{\partial x},\\
&\frac{\partial v}{\partial t}+fu=-\frac{1}{\rho_0}\frac{\partial p}{\partial y},\\
&\frac{\partial w}{\partial t}=-\frac{1}{\rho_0}\frac{\partial p}{\partial z}-\frac{\rho g}{\rho_0},\\
&\frac{\partial \rho}{\partial t}-\frac{\rho_0 N^2}{g}w=0.
\end{aligned} \tag{13.95}$$

We have not made the hydrostatic assumption because we are *not* assuming that the horizontal wavelength is long compared to the vertical wavelength. The advective term in the density equation is written in a linearized form $w(d\overline{\rho}/dz) = -\rho_0 N^2 w/g$. Thus the rate of change of density at a point is assumed to be due only to the vertical advection of the background density distribution $\overline{\rho}(z)$. Because internal wave activity is more intense in the thermocline where N varies appreciably (Figure 13.2), we shall be somewhat more general than in Chapter 7 and let N be depth independent.

An equation for w can be formed from the set (13.95) by eliminating all other variables. The algebraic steps of such a procedure are shown in Section 7.8 without the Coriolis forces. This gives

$$\frac{\partial^2}{\partial t^2}\nabla^2 w + N^2\nabla_{\mathrm{H}}^2 w + f^2\frac{\partial^2 w}{\partial z^2} = 0, \tag{13.96}$$

where $\nabla^2 \equiv \partial^2/\partial x^2 + \partial^2/\partial y^2 + \partial^2/\partial z^2$ and $\nabla_{\mathrm{H}}^2 \equiv \partial^2/\partial x^2 + \partial^2/\partial y^2$. Because the coefficients in (13.96) are independent of the horizontal directions, equation (13.96) can have solutions that are trigonometric in x and y. We therefore assume a solution of the form

$$[u, v, w] = [\widehat{u}\,(z), \widehat{v}(z), \widehat{w}(z)]\, e^{i(kx+ly-\omega t)}. \tag{13.97}$$

Substitution into (13.96) gives

$$(-i\omega)^2\left[(ik)^2 + (il)^2 + \frac{d^2}{dz^2}\right]\widehat{w} + N^2\left[(ik)^2 + (il)^2\right]\widehat{w} + f^2\frac{d^2\widehat{w}}{dz^2} = 0,$$

from which we obtain

$$\frac{d^2\widehat{w}}{dz^2} + \frac{(N^2-\omega^2)(k^2+l^2)}{\omega^2 - f^2}\widehat{w} = 0. \tag{13.98}$$

Defining

$$m^2(z) \equiv \frac{(k^2+l^2)[N^2(z)-\omega^2]}{\omega^2 - f^2}, \tag{13.99}$$

equation (13.98) becomes

$$\frac{d^2\widehat{w}}{dz^2} + m^2\widehat{w} = 0. \tag{13.100}$$

For $m^2 < 0$, the solutions of (13.100) are exponential in z signifying that the resulting motion is surface-trapped. It represents a surface wave propagating horizontally. For a positive m^2, on the other hand, solutions are trigonometric in z, giving internal waves propagating vertically as well as horizontally. From (13.99), therefore, internal waves are possible only in the frequency range:

$$f < \omega < N,$$

where we have assumed $N > f$, as is true for much of the atmosphere and the ocean.

WKB Solution

To proceed further, we assume that $N(z)$ is a slowly varying function in that its fractional change over a vertical wavelength is much less than unity. We are therefore considering only those internal waves whose vertical wavelength is short compared to the scale of variation of N. If H is a characteristic vertical distance over which N varies appreciably, then we are assuming that

$$Hm \gg 1.$$

For such slowly varying $N(z)$, we expect that $m(z)$ given by (13.99) is also a slowly varying function, that is, $m(z)$ changes by a small fraction in a distance $1/m$. Under this assumption the waves *locally* behave like plane waves, as if m is constant. This is the so-called *WKB approximation* (after Wentzel-Kramers-Brillouin), which applies when the properties of the medium (in this case N) are slowly varying.

To derive the approximate WKB solution of equation (13.100), we look for a solution in the form

$$\widehat{w} = A(z)e^{i\phi(z)},$$

where the phase ϕ and the (slowly varying) amplitude A are real. (No generality is lost by assuming A to be real. Suppose it is complex and of the form $A = \overline{A}exp(i\alpha)$, where $\overline{A}$ and α are real. Then $\widehat{w} = \overline{A}exp\,[i(\phi + \alpha)]$, a form in which $(\phi + \alpha)$ is the phase.) Substitution into (13.100) gives

$$\frac{d^2A}{dz^2} + A\left[m^2 - \left(\frac{d\phi}{dz}\right)^2\right] + i2\frac{dA}{dz}\frac{d\phi}{dz} + iA\frac{d^2\phi}{dz^2} = 0.$$

Equating the real and imaginary parts, we obtain

$$\frac{d^2A}{dz^2} + A\left[m^2 - \left(\frac{d\phi}{dz}\right)^2\right] = 0, \quad 2\frac{dA}{dz}\frac{d\phi}{dz} + A\frac{d^2\phi}{dz^2} = 0. \tag{13.101, 13.102}$$

In (13.101) the term $d^2\mathrm{A}/dz^2$ is negligible because its ratio with the second term is

$$\frac{d^2A/dz^2}{Am^2} \sim \frac{1}{H^2m^2} \ll 1.$$

Equation (13.101) then becomes approximately

$$\frac{d\phi}{dz} = \pm m, \tag{13.103}$$

whose solution is

$$\phi = \pm \int^z m\,dz,$$

the lower limit of the integral being arbitrary.

The amplitude is determined by writing (13.102) in the form

$$\frac{dA}{A} = -\frac{(d^2\phi/dz^2)dz}{2(d\phi/dz)} = -\frac{(dm/dz)dz}{2m} = -\frac{1}{2}\frac{dm}{m},$$

where (13.103) has been used. Integrating, we obtain $\ln A = -\frac{1}{2}\ln m + \text{const.}$, that is,

$$A = \frac{A_0}{\sqrt{m}},$$

where A_0 is a constant. The WKB solution of (13.100) is therefore

$$\widehat{w} = \frac{A_0}{\sqrt{m}} e^{\pm i\int^z m\,dz}. \tag{13.104}$$

Because of neglect of the β-effect, the waves must behave similarly in x and y, as indicated by the symmetry of the dispersion relation (13.99) in k and l. Therefore, we lose no generality by orienting the x-axis in the direction of propagation and taking:

$$k > 0 \quad l = 0 \quad \omega > 0.$$

To find u and v in terms of w, use the continuity equation $\partial u/\partial x + \partial w/\partial z = 0$, noting that the y-derivatives are zero because of our setting $l = 0$. Substituting the wave solution (13.97) into the continuity equation gives

$$ik\widehat{u} + \frac{d\widehat{w}}{dz} = 0. \tag{13.105}$$

The z-derivative of $\widehat{w}$ in (13.104) can be obtained by treating the denominator $\sqrt{m}$ as approximately constant because the variation of $\widehat{w}$ is dominated by the wiggly behavior of the local plane wave solution. This gives

$$\frac{d\widehat{w}}{dz} = \frac{A_0}{\sqrt{m}}(\pm im)e^{\pm i\int^z m\,dz} = \pm iA_0\sqrt{m}e^{\pm i\int^z m\,dz},$$

so that equation (13.105) becomes

$$\widehat{u} = \mp\frac{A_0\sqrt{m}}{k} e^{\pm i\int^z m\,dz}. \tag{13.106}$$

An expression for $\widehat{v}$ can now be obtained from the horizontal equations of motion in (13.95). Cross differentiating, we obtain the vorticity equation

$$\frac{\partial}{\partial t}\left(\frac{\partial u}{\partial y} - \frac{\partial v}{\partial x}\right) = f\left(\frac{\partial u}{\partial x} + \frac{\partial v}{\partial y}\right).$$

Using the wave solution (13.97), this gives

$$\frac{\widehat{u}}{\widehat{v}} = \frac{i\omega}{f}.$$

Equation (13.106) then gives

$$\hat{v} = \pm\frac{if}{\omega}\frac{A_0\sqrt{m}}{k}e^{\pm i\int^z m\,dz}. \tag{13.107}$$

Taking real parts of equations (13.104), (13.106), and (13.107), we obtain the velocity field:

$$\begin{aligned} u &= \mp\frac{A_0\sqrt{m}}{k}\cos\left(kx \pm \int^z m\,dz - \omega t\right), \\ v &= \mp\frac{A_0 f\sqrt{m}}{\omega k}\sin\left(kx \pm \int^z m\,dz - \omega t\right), \\ w &= \frac{A_0}{\sqrt{m}}\cos\left(kx \pm \int^z m\,dz - \omega t\right), \end{aligned} \tag{13.108}$$

where the dispersion relation is

$$m^2 = \frac{k^2(N^2-\omega^2)}{\omega^2 - f^2}. \tag{13.109}$$

The meaning of $m(z)$ is clear from (13.108). If we call the argument of the trigonometric terms the *phase*, then it is apparent that $\partial(phase)/\partial z = m(z)$, so that $m(z)$ is the *local* vertical wave number. Because we are treating k, m, $\omega > 0$, it is also apparent that the *upper signs represent waves with upward phase propagation, and the lower signs represent downward phase propagation*.

Particle Orbit

To find the shape of the hodograph in the horizontal plane, consider the point $x = z = 0$. Then (13.108) gives:

$$\begin{aligned} u &= \mp\cos\omega t, \\ v &= \pm\frac{f}{\omega}\sin\omega t, \end{aligned} \tag{13.110}$$

where the amplitude of u has been arbitrarily set to one. Taking the upper signs in (13.110), the values of u and v are indicated in Figure 13.22a for three values of time corresponding to $\omega t = 0$, $\pi/2$, and π. It is clear that the horizontal hodographs are clockwise ellipses, with the major axis in the direction of propagation x, and the axis ratio is f/ω. The same conclusion applies for the lower signs in (13.110). The particle orbits in the horizontal plane are therefore identical to those of Poincaré waves (Figure 13.15).

However, the plane of the motion is no longer horizontal. From the velocity components equation (13.108), we note that

$$\frac{u}{w} = \mp\frac{m}{k} = \mp\tan\theta, \tag{13.111}$$

where $\theta = \tan^{-1}(m/k)$ is the angle made by the wave number vector $\mathbf{K}$ with the horizontal (Figure 13.23). For upward phase propagation, equation (13.111) gives $u/w = -\tan\theta$, so that w is negative if u is positive, as indicated in Figure 13.23. A three-dimensional sketch of the particle orbit is shown in Figure 13.22b. It is easy to show (Exercise 13.6) that the phase

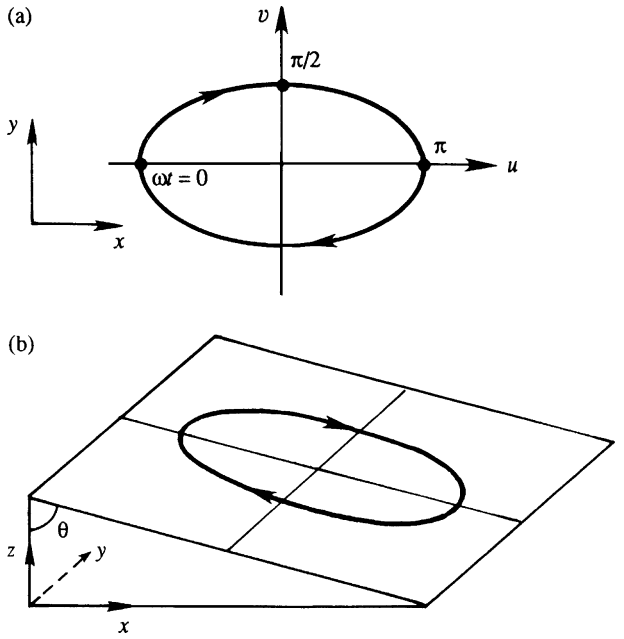

FIGURE 13.22 Particle orbit in an internal wave having x-direction wave number $k \neq 0$, and y-direction wave number $l = 0$. The upper panel (a) shows a projection on a horizontal plane; points corresponding to $\omega t = 0, \pi/2$, and π are indicated. The sense of rotation is the same as that of the surface-gravity-wave particle orbit shown in Figure 13.15 and is valid for the northern hemisphere. The lower panel (b) shows a three-dimensional view of the orbit.

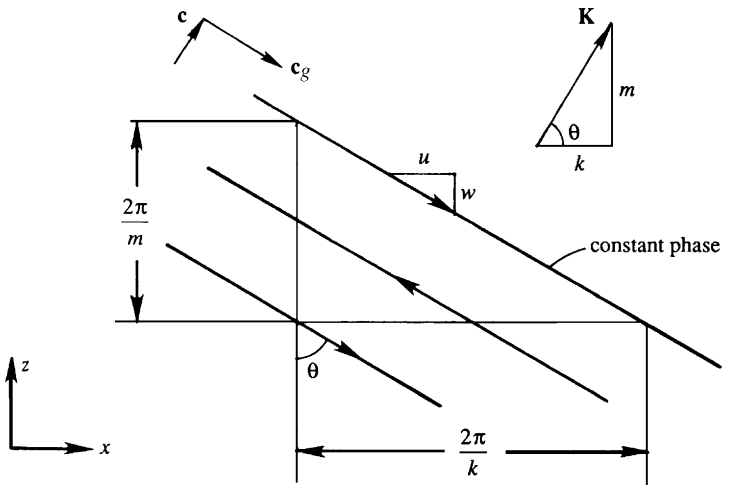

FIGURE 13.23 Vertical section of an internal wave. The three parallel lines are constant phase lines corresponding to one full wavelength, with the arrows indicating fluid motion along the lines. The phase velocity is perpendicular to the crests. The group velocity is parallel to the crests. The angle θ of the wave number with respect to the horizontal depends on the wave frequency ω, the buoyancy frequency N, and the local inertial frequency f.

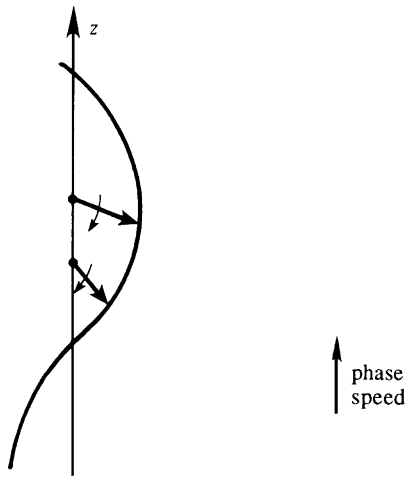

FIGURE 13.24 Helical-spiral traced out by the tips of instantaneous velocity vectors in an internal wave with upward phase speed. Heavy arrows show the velocity vectors at two depths, and light arrows indicate that they are rotating clockwise with increasing time. Note that the instantaneous vectors turn clockwise with increasing depth.

velocity vector **c** is in the direction of **K**, that **c** and $\mathbf{c}_g$ are perpendicular, and that the fluid motion **u** is parallel to $\mathbf{c}_g$; these facts are discussed in Chapter 7 for internal waves unaffected by Coriolis forces.

The velocity vector at any location rotates clockwise with time. Because of the vertical propagation of phase, the tips of the *instantaneous* vectors also turn with *depth*. Consider the turning of the velocity vectors with depth when the phase velocity is upward, so that the deeper currents have a phase lead over the shallower currents (Figure 13.24). Because the currents at all depths rotate clockwise in *time* (whether the vertical component of **c** is upward or downward), it follows that the tips of the instantaneous velocity vectors should fall on a helical spiral that turns clockwise with *depth*. Only such a turning in depth, coupled with a clockwise rotation of the velocity vectors with time, can result in a phase lead of the deeper currents. In the opposite case of a *downward* phase propagation, the helix turns *counterclockwise* with depth. The direction of turning of the velocity vectors can also be found from (13.108), by considering $x = t = 0$ and finding u and v at various values of z.

Discussion of the Dispersion Relation

The dispersion relation (13.109) can be written as

$$\omega^2 - f^2 = \frac{k^2}{m^2}(N^2 - \omega^2). \tag{13.112}$$

Introducing $\tan\theta = m/k$, (13.112) becomes

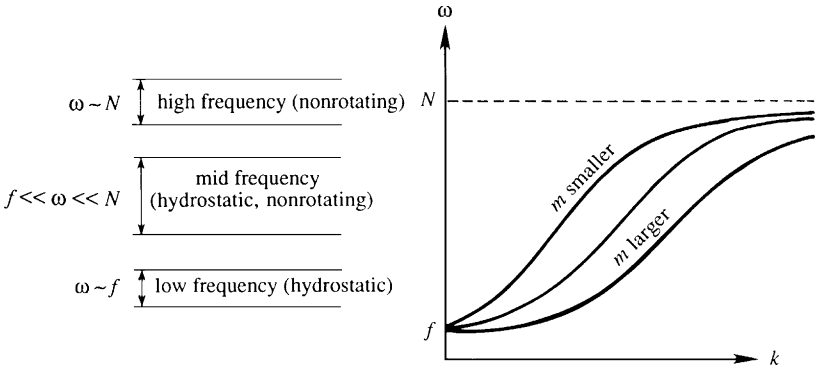

FIGURE 13.25 Dispersion relation for internal waves. The different regimes are indicated on the left-hand side of the figure. The wave frequency ω increases monotonically with increasing horizontal wave number k. The buoyancy frequency N and the local inertial frequency f set the upper and lower limits for ω.

$$\omega^2 = f^2 \sin^2\theta + N^2 \cos^2\theta,$$

which shows that ω is a function of the angle made by the wave number with the horizontal and is not a function of the magnitude of $\mathbf{K}$. For $f = 0$ the aforementioned expression reduces to $\omega = N \cos\theta$, derived in Section 7.8 without Coriolis forces.

A plot of the dispersion relation (13.112) is presented in Figure 13.25, showing ω as a function of k for various values of m. All curves pass through the point $\omega = f$, which represents inertial oscillations. Typically, $N \gg f$ in most of the atmosphere and the ocean. Because of the wide separation of the upper and lower limits of the internal wave range $f \leq \omega \leq N$, various limiting cases are possible, as indicated in Figure 13.25. They are

(1) *High-frequency regime* ($\omega \sim N$, *but* $\omega \leq N$): In this range f^2 is negligible in comparison with ω^2 in the denominator of the dispersion relation (13.109), which reduces to:

$$m^2 \simeq \frac{k^2(N^2 - \omega^2)}{\omega^2}, \quad \text{that is,} \quad \omega^2 \simeq \frac{N^2 k^2}{m^2 + k^2}.$$

Using $\tan\theta = \mathrm{m/k}$, this gives $\omega = N \cos\theta$. Thus, the high-frequency internal waves are the same as the nonrotating internal waves discussed in Chapter 7.

(2) *Low-frequency regime* ($\omega \sim f$, *but* $\omega \geq f$): In this range ω^2 can be neglected in comparison to N^2 in the dispersion relation (13.109), which becomes:

$$m^2 \simeq \frac{k^2 N^2}{\omega^2 - f^2}, \quad \text{that is,} \quad \omega^2 \simeq f^2 + \frac{k^2 N^2}{m^2}.$$

The low-frequency limit is obtained by making the hydrostatic assumption, that is, neglecting $\partial w/\partial t$ in the vertical equation of motion.

(3) *Mid-frequency regime* ($f \ll \omega \ll N$): In this range the dispersion relation (13.109) simplifies to

$$m^2 \simeq \frac{k^2 N^2}{\omega^2},$$

so that *both* the hydrostatic and the nonrotating assumptions are applicable.

Lee Wave

Internal waves are frequently found in the *lee* (that is, the downstream side) of mountains. In stably stratified conditions, the flow of air over a mountain causes a vertical displacement of fluid particles, which sets up internal waves as it moves downstream of the mountain. If the amplitude is large and the air is moist, the upward motion causes condensation and cloud formation.

Due to the effect of a mean flow, the lee waves are stationary with respect to the ground. This is shown in Figure 13.26, where the westward phase speed is canceled by the eastward mean flow. We shall determine what wave parameters make this cancellation possible. The frequency of lee waves is much larger than f, so that rotational effects are negligible. The dispersion relation is therefore

$$\omega^2 = \frac{N^2 k^2}{m^2 + k^2}. \tag{13.113}$$

However, we now have to introduce the effects of the mean flow. The dispersion relation (13.113) is still valid if ω is interpreted as the *intrinsic frequency,* that is, the frequency measured in a frame of reference moving with the mean flow. In a medium moving with a velocity $\mathbf{U}$, the *observed frequency* of waves at a fixed point is Doppler shifted to

$$\omega_0 = \omega + \mathbf{K}\cdot\mathbf{U},$$

where ω is the intrinsic frequency; this is discussed further in Section 7.1. For a stationary wave $\omega_0 = 0$, which requires that the intrinsic frequency is $\omega = -\mathbf{K}\cdot\mathbf{U} = kU$. (Here $-\mathbf{K}\cdot\mathbf{U}$ is

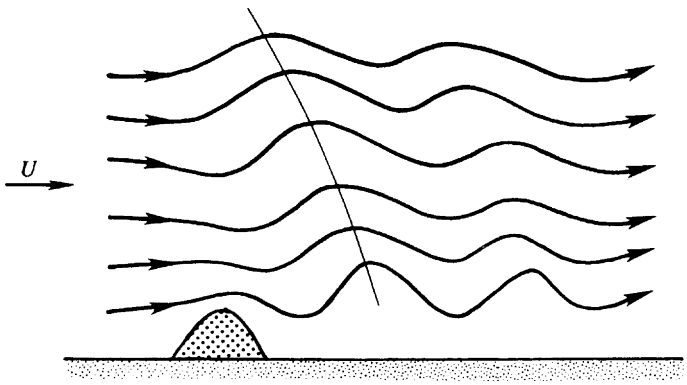

FIGURE 13.26 Schematic streamlines in a lee wave downstream of a mountain. The thin line drawn through crests shows that the phase propagates downward and westward when the eastward velocity U is accounted for.

positive because **K** is westward and **U** is eastward.) The dispersion relation (13.113) then gives

$$U = \frac{N}{\sqrt{k^2 + m^2}}.$$

If the flow speed U is given, and the mountain introduces a typical horizontal wave number k, then the preceding equation determines the vertical wave number m that generates stationary waves. Waves that do not satisfy this condition would radiate away.

The energy source of lee waves is at the surface. The energy therefore must propagate upward, and consequently the phases propagate downward. The intrinsic phase speed is therefore westward and downward in Figure 13.26. With this information, we can determine which way the constant phase lines should tilt in a stationary lee wave. Note that the wave pattern in Figure 13.26 would propagate to the left in the absence of a mean velocity, and only with the constant phase lines tilting backward with height would the flow at larger height lead the flow at a lower height.

Further discussion of internal waves can be found in Phillips (1977) and Munk (1981); lee waves are discussed in Holton (1979).

13.15. ROSSBY WAVE

To this point we have discussed wave motions that are possible with a constant Coriolis frequency f and found that these waves have frequencies larger than f. We shall now consider wave motions that owe their existence to the variation of f with latitude. With such a variable f, the equations of motion allow a very important type of wave motion called the *Rossby wave*. Their spatial scales are so large in the atmosphere that they usually have only a few wavelengths around the entire globe (Figure 13.27). This is why Rossby waves are also called *planetary waves*. In the ocean, however, their wavelengths are only about 100 km. Rossby-wave frequencies obey the inequality $\omega \ll f$. Because of this slowness the time derivative terms are an order of magnitude smaller than the Coriolis acceleration and the pressure gradients in the horizontal equations of motion. Such *nearly* geostrophic flows are called *quasi-geostrophic motions*.

Quasi-Geostrophic Vorticity Equation

We shall first derive the governing equation for quasi-geostrophic motions. For simplicity, we shall make the customary β-plane approximation valid for $\beta y \ll f_0$, keeping in mind that the approximation is not a good one for atmospheric Rossby waves, which have planetary scales. Although Rossby waves are frequently superposed on a mean flow, we shall derive the equations without a mean flow, and superpose a uniform mean flow at the end, assuming that the perturbations are small and that a linear superposition is valid. The first step is to simplify the vorticity equation for quasi-geostrophic motions, assuming that the *velocity is geostrophic to the lowest order*. The small departures from geostrophy, however, are important because they determine the *evolution* of the flow with time.

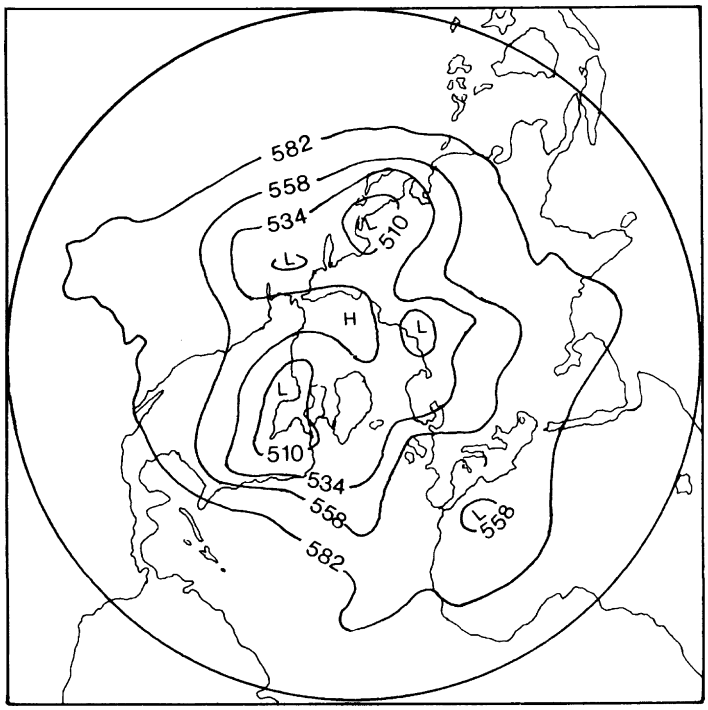

FIGURE 13.27 Observed height (in decameters = km/100) of the 50 kPa pressure surface in the northern hemisphere. The center of the picture represents the north pole. The undulations are due to Rossby waves. *J. T. Houghton,* The Physics of the Atmosphere, *1986; reprinted with the permission of Cambridge University Press.*

We start with the shallow-water potential vorticity equation:

$$\frac{D}{Dt}\left(\frac{\zeta + f}{h}\right) = 0,$$

which can be written as

$$h\frac{D}{Dt}(\zeta + f) - (\zeta + f)\frac{Dh}{Dt} = 0.$$

We now expand the material derivative and substitute $h = H + \eta$, where H is the uniform undisturbed depth of the layer, and η is the surface displacement. This gives

$$(H + \eta)\left(\frac{\partial \zeta}{\partial t} + u\frac{\partial \zeta}{\partial x} + v\frac{\partial \zeta}{\partial y} + \beta v\right) - (\zeta + f_0)\left(\frac{\partial \eta}{\partial t} + u\frac{\partial \eta}{\partial x} + v\frac{\partial \eta}{\partial y}\right) = 0. \tag{13.114}$$

Here, we have used $Df/Dt = v(df/dy) = \beta v$. We have also replaced f by f_0 in the second term because the β-plane approximation neglects the variation of f *except* when it involves df/dy. For small perturbations we can neglect the quadratic nonlinear terms in (13.114), obtaining

$$H\frac{\partial \zeta}{\partial t} + H\beta v - f_0\frac{\partial \eta}{\partial t} = 0. \tag{13.115}$$

This is the linearized form of the potential vorticity equation. Its quasi-geostrophic version is obtained if we substitute the approximate geostrophic expressions for velocity:

$$u \simeq -\frac{g}{f_0}\frac{\partial \eta}{\partial y}, \qquad v \simeq \frac{g}{f_0}\frac{\partial \eta}{\partial x}. \tag{13.116}$$

From this the vorticity is found as

$$\zeta = \frac{g}{f_0}\left(\frac{\partial^2 \eta}{\partial x^2} + \frac{\partial^2 \eta}{\partial y^2}\right),$$

so that the vorticity equation (13.115) becomes

$$\frac{gH}{f_0}\frac{\partial}{\partial t}\left(\frac{\partial^2 \eta}{\partial x^2} + \frac{\partial^2 \eta}{\partial y^2}\right) + \frac{gH\beta}{f_0}\frac{\partial \eta}{\partial x} - f_0\frac{\partial \eta}{\partial t} = 0.$$

Denoting $c = \sqrt{gH}$, this becomes

$$\frac{\partial}{\partial t}\left(\frac{\partial^2 \eta}{\partial x^2} + \frac{\partial^2 \eta}{\partial y^2} - \frac{f_0^2}{c^2}\eta\right) + \beta\frac{\partial \eta}{\partial x} = 0. \tag{13.117}$$

This is the quasi-geostrophic form of the linearized vorticity equation, which governs the flow of large-scale motions. The ratio c/f_0 is recognized as the Rossby radius. Note that we have not set $\partial\eta/\partial t = 0$ in (13.115) during the derivation of (13.117), although a strict validity of the geostrophic relations (13.116) would require that the horizontal divergence, and hence $\partial\eta/\partial t$, be zero. This is because the *departure* from strict geostrophy determines the evolution of the flow described by (13.117). We can therefore use the geostrophic relations for velocity everywhere except in the horizontal divergence term in the vorticity equation.

Dispersion Relation

Assume solutions of the form:

$$\eta = \hat{\eta}\, e^{i(kx+ly-\omega t)}.$$

We shall regard ω as positive; the signs of k and l then determine the direction of phase propagation. A substitution into the vorticity equation (13.117) gives

$$\omega = -\frac{\beta k}{k^2 + l^2 + f_0^2/c^2}. \tag{13.118}$$

This is the dispersion relation for *Rossby waves*. The asymmetry of the dispersion relation with respect to k and l signifies that the wave motion is not isotropic in the horizontal, which is expected because of the β-effect. Although we have derived it for a single homogeneous layer, it is equally applicable to stratified flows if c is replaced by the corresponding *internal*

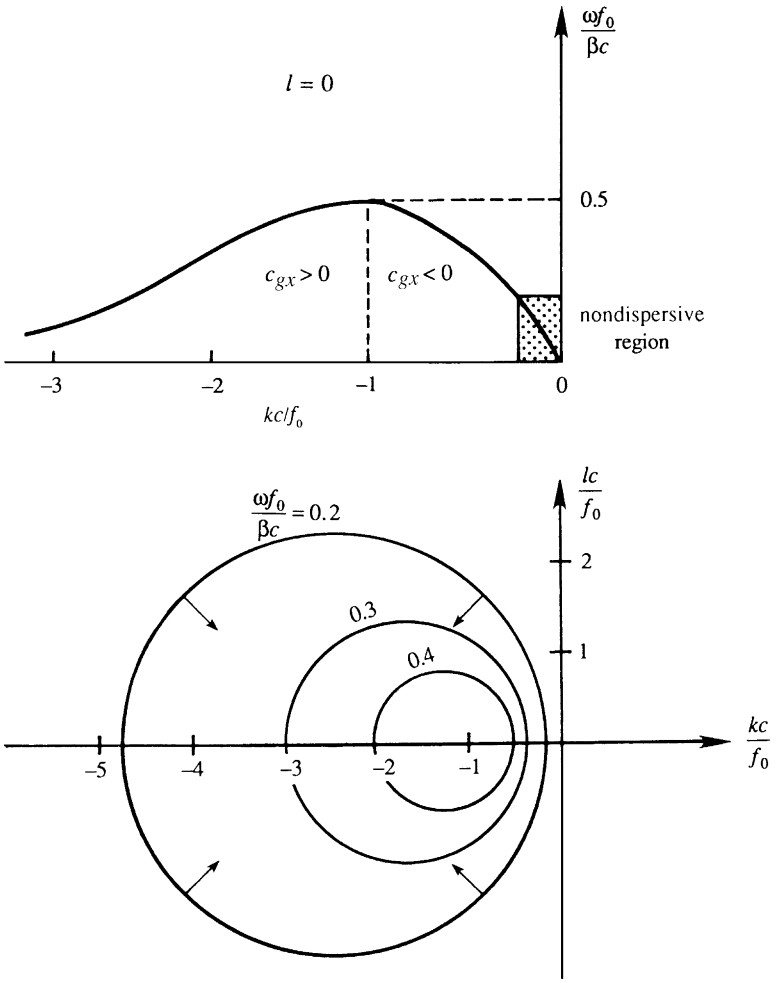

FIGURE 13.28 Dispersion relation $\omega(k,l)$ for a Rossby wave. The upper panel shows ω versus k for $l = 0$. Regions of positive and negative group velocity c_{gx} are indicated. The lower panel shows a plane view of the surface $\omega(k,l)$, showing contours of constant ω on a kl-plane. The values of $\omega f_0/\beta c$ for the three circles are 0.2, 0.3, and 0.4. Arrows perpendicular to ω contours indicate directions of group velocity vector $\mathbf{c}_g$. *A. E. Gill,* Atmosphere−Ocean Dynamics, *1982; reprinted with the permission of Academic Press and Mrs. Helen Saunders-Gill.*

value, which is $c = \sqrt{g'H}$ for the reduced-gravity model (see Section 7.7) and $c = NH/n\pi$ for the nth mode of a continuously stratified model. For the barotropic mode c is very large, and f_0^2/c^2 is usually negligible in the denominator of (13.118).

The dispersion relation $\omega(k,l)$ in (13.118) can be displayed as a surface, taking k and l along the horizontal axes and ω along the vertical axis. The section of this surface along $l = 0$ is indicated in the upper panel of Figure 13.28, and sections of the surface for three values of ω are indicated in the bottom panel. The contours of constant ω are circles because the dispersion relation (13.118) can be written as

$$\left(k + \frac{\beta}{2\omega}\right)^2 + l^2 = \left(\frac{\beta}{2\omega}\right)^2 - \frac{f_0^2}{c^2}.$$

The definition of group velocity,

$$\boldsymbol{c}_g = \mathbf{e}_x \frac{\partial \omega}{\partial k} + \mathbf{e}_y \frac{\partial \omega}{\partial l},$$

shows that the group velocity vector is the gradient of ω in the wave number space. The direction of $\mathbf{c}_g$ is therefore perpendicular to the ω contours, as indicated in the lower panel of Figure 13.28. For $l = 0$, the maximum frequency and zero group speed are attained at $kc/f_0 = -1$, corresponding to $\omega_{\max} f_0/\beta c = 0.5$. The maximum frequency is much smaller than the Coriolis frequency. For example, in the ocean the ratio $\omega_{max}/f_0 = 0.5\beta c/f_0^2$ is of order 0.1 for the barotropic mode, and of order 0.001 for a baroclinic mode, taking a typical mid-latitude value of $f_0 \sim 10^{-4}$ s^{-1}, a barotropic gravity wave speed of $c \sim 200$ m/s, and a baroclinic gravity wave speed of $c \sim 2$ m/s. The shortest period of mid-latitude baroclinic Rossby waves in the ocean can therefore be more than a year.

The eastward phase speed is

$$c_x = \frac{\omega}{k} = -\frac{\beta}{k^2 + l^2 + f_0^2/c^2}. \tag{13.119}$$

The negative sign shows that the *phase propagation is always westward*. The phase speed reaches a maximum when $k^2 + l^2 \to 0$, corresponding to very large wavelengths represented by the region near the origin of Figure 13.28. In this region the waves are nearly nondispersive and have an eastward phase speed:

$$c_x \simeq -\frac{\beta c^2}{f_0^2}.$$

With $\beta = 2 \times 10^{-11}$ m^{-1} s^{-1}, a typical baroclinic value of $c \sim 2$ m/s, and a mid-latitude value of $f_0 \sim 10^{-4}$ s^{-1}, this gives $c_x \sim 10^{-2}$ m/s. At these slow speeds the Rossby waves would take years to cross the width of the ocean at mid-latitudes. The Rossby waves in the ocean are therefore more important at lower latitudes, where they propagate faster. (The dispersion relation (13.118), however, is not valid within a latitude band of 3° from the equator, for then the assumption of a near geostrophic balance breaks down. A different analysis is needed in the tropics. A discussion of the wave dynamics of the tropics is given in Gill (1982) and in the review paper by McCreary (1985).) In the atmosphere c is much larger, and consequently the Rossby waves propagate faster. A typical large atmospheric disturbance can propagate as a Rossby wave at a speed of several meters per second.

Frequently, the Rossby waves are superposed on a strong eastward mean current, such as the atmospheric jet stream. If U is the speed of this eastward current, then the observed eastward phase speed is

$$c_x = U - \frac{\beta}{k^2 + l^2 + f_0^2/c^2}. \tag{13.120}$$

Stationary Rossby waves can therefore form when the eastward current cancels the westward phase speed, giving $c_x = 0$. This is how stationary waves are formed downstream of the topographic step in Figure 13.20. A simple expression for the wavelength results if we assume

$l = 0$ and the flow is barotropic, so that f_0^2/c^2 is negligible in (13.120). This gives $U = \beta/k^2$ for stationary solutions, so that the wavelength is $2\pi\sqrt{U/\beta}$.

Finally, note that we have been rather cavalier in deriving the quasi-geostrophic vorticity equation in this section, in the sense that we have substituted the approximate geostrophic expressions for velocity without a formal ordering of the scales. Gill (1982) has given a more precise derivation, expanding in terms of a small parameter. Another way to justify the dispersion relation (13.118) is to obtain it from the general dispersion relation (13.76) derived in Section 13.10:

$$\omega^3 - c^2\omega(k^2 + l^2) - f_0^2\omega - c^2\beta k = 0. \tag{13.121}$$

For $\omega \ll f$, the first term is negligible compared to the third, reducing (13.121) to (13.118).

13.16. BAROTROPIC INSTABILITY

In Section 11.9 we discussed the inviscid stability of a shear flow $U(y)$ in a nonrotating system, and demonstrated that a necessary condition for its instability is that d^2U/dy^2 must change sign somewhere in the flow. This was called *Rayleigh's inflection point criterion*. In terms of vorticity $\overline{\zeta} = -dU/dy$, the criterion states that $d\overline{\zeta}/dy$ must change sign somewhere in the flow. We shall now show that, on a rotating earth, the criterion requires that $d(\overline{\zeta} + f)/dy$ must change sign somewhere within the flow.

Consider a horizontal current $U(y)$ in a medium of uniform density. In the absence of horizontal density gradients only the barotropic mode is allowed, and $U(y)$ does not vary with depth. The vorticity equation is

$$\left(\frac{\partial}{\partial t} + \mathbf{u}\cdot\nabla\right)(\zeta + f) = 0. \tag{13.122}$$

This is identical to the potential vorticity equation $D/Dt[(\zeta + f)/h] = 0$, with the added simplification that the layer depth is constant because $w = 0$. Let the total flow be decomposed into background flow plus a disturbance:

$$\begin{aligned} u &= U(y) + u', \\ v &= v'. \end{aligned}$$

The total vorticity is then

$$\zeta = \overline{\zeta} + \zeta' = -\frac{dU}{dy} + \left(\frac{\partial v'}{\partial x} - \frac{\partial u'}{\partial y}\right) = -\frac{dU}{dy} + \nabla^2\psi,$$

where we have defined the perturbation stream function:

$$u' = -\frac{\partial \psi}{\partial y'}, \qquad v' = \frac{\partial \psi}{\partial x}.$$

Substituting into (13.122) and linearizing, we obtain the perturbation vorticity equation:

$$\frac{\partial}{\partial t}(\nabla^2\psi) + U\frac{\partial}{\partial x}(\nabla^2\psi) + \left(\beta - \frac{d^2U}{dy^2}\right)\frac{\partial\psi}{\partial x} = 0. \tag{13.123}$$

Because the coefficients of (13.123) are independent of x and t, there can be solutions of the form:

$$\psi = \widehat{\psi}(y)\, e^{ik(x-ct)}.$$

The phase speed c is complex and solutions are unstable if its imaginary part $c_i > 0$. The perturbation vorticity equation (13.123) then becomes

$$(U-c)\left[\frac{d^2}{dy^2} - k^2\right]\widehat{\psi} + \left[\beta - \frac{d^2U}{dy^2}\right]\widehat{\psi} = 0.$$

Comparing this with (11.81) derived without Coriolis forces, it is seen that the effect of planetary rotation is the replacement of $-d^2U/dy^2$ by $(\beta - d^2U/dy^2)$. The analysis of the section therefore carries over to the present case, resulting in the following criterion: *A necessary condition for the inviscid instability of a barotropic current $U(y)$ is that the gradient of the absolute vorticity,*

$$\frac{d}{dy}(\overline{\zeta} + f) = \beta - \frac{d^2U}{dy^2}, \tag{13.124}$$

must change sign somewhere in the flow. This result was first derived by Kuo (1949).

Barotropic instability quite possibly plays an important role in the instability of currents in the atmosphere and in the ocean. The instability has no preference for any latitude, because

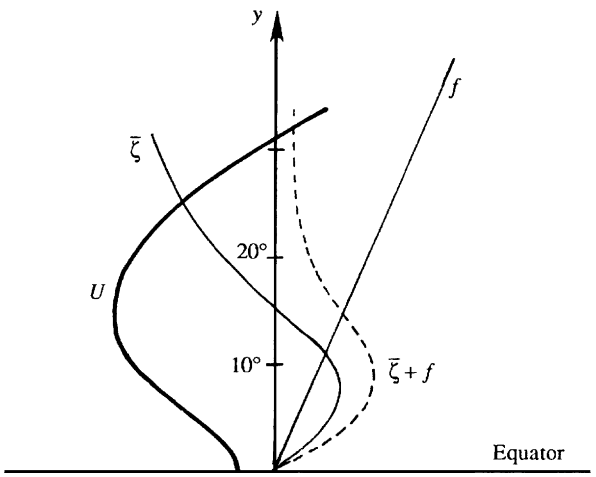

FIGURE 13.29 Profiles of velocity and vorticity in a westward tropical wind. The velocity distribution is barotropically unstable as $d(\overline{\zeta}+f)/dy$ (shown as the dashed curve) changes sign within the flow. *J. T. Houghton,* The Physics of the Atmosphere, *1986; reprinted with the permission of Cambridge University Press.*

the criterion involves β and not f. However, the mechanism presumably dominates in the tropics because mid-latitude disturbances prefer the *baroclinic instability* mechanism discussed in the following section. An unstable distribution of westward tropical wind is shown in Figure 13.29.

13.17. BAROCLINIC INSTABILITY

The weather maps at mid-latitudes invariably show the presence of wavelike horizontal excursions of temperature and pressure contours, superposed on eastward mean flows such as the jet stream. Similar undulations are also found in the ocean on eastward currents such as the Gulf Stream in the north Atlantic. A typical wavelength of these disturbances is observed to be of the order of the internal Rossby radius, that is, about 4000 km in the atmosphere and 100 km in the ocean. They seem to be propagating as Rossby waves, but their erratic and unexpected appearance suggests that they are not forced by any external agency, but are due to an inherent *instability* of mid-latitude eastward flows. In other words, the eastward flows have a spontaneous tendency to develop wavelike disturbances. In this section we shall investigate the instability mechanism that is responsible for the spontaneous relaxation of eastward jets into a meandering state.

The poleward decrease of the solar irradiation results in a poleward decrease of air temperature and a consequent increase of air density. An idealized distribution of the atmospheric density in the northern hemisphere is shown in Figure 13.30. The density increases northward due to the lower temperatures near the poles and decreases upward because of static stability. According to the thermal wind relation (13.15), an eastward flow (such as the jet stream in the atmosphere or the Gulf Stream in the Atlantic) in equilibrium with such a density structure must have a velocity that increases with height. A system with inclined density surfaces, such as the one in Figure 13.30, has more potential energy than a system with horizontal density surfaces, just as a system with an inclined free surface has more potential energy than a system with a horizontal free surface. It is therefore potentially unstable because it can release the stored potential energy by means of an instability that would cause the density surfaces to flatten out. In the process, vertical shear of the mean flow $U(z)$ would decrease, and perturbations would gain kinetic energy.

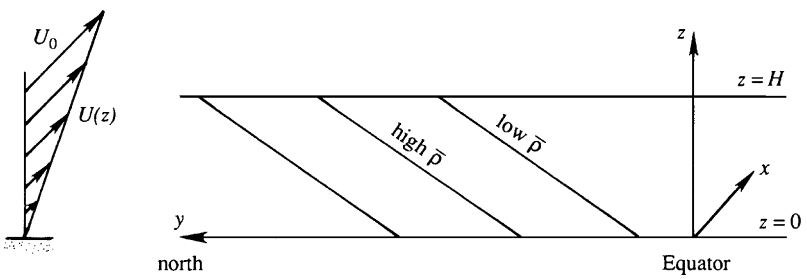

FIGURE 13.30 Lines of constant density in the northern hemispheric atmosphere. The lines are nearly horizontal and the slopes are greatly exaggerated in the figure. The velocity $U(z)$ shown at the left is into the plane of paper.

Instability of baroclinic jets that release potential energy by flattening out the density surfaces is called the *baroclinic instability*. Our analysis would show that the preferred scale of the unstable waves is indeed of the order of the Rossby radius, as observed for the mid-latitude weather disturbances. The theory of baroclinic instability was developed in the 1940s by Vilhem Bjerknes and others, and is considered one of the major triumphs of geophysical fluid mechanics. Our presentation is essentially based on the review article by Pedlosky (1971).

Consider a basic state in which the density is stably stratified in the vertical with a *uniform* buoyancy frequency N, and increases northward at a *constant* rate $\partial\overline{\rho}/\partial y$. According to the thermal wind relation, the constancy of $\partial\overline{\rho}/\partial y$ requires that the vertical shear of the basic eastward flow $U(z)$ also be constant. The β-effect is neglected as it is not an essential requirement of the instability. (The β-effect does modify the instability, however.) This is borne out by the spontaneous appearance of undulations in laboratory experiments in a rotating annulus, in which the inner wall is maintained at a higher temperature than the outer wall. The β-effect is absent in such an experiment.

Perturbation Vorticity Equation

The equations for total flow are:

$$\begin{aligned}
&\frac{\partial u}{\partial t}+u\frac{\partial u}{\partial x}+v\frac{\partial u}{\partial y}-fv = -\frac{1}{\rho_0}\frac{\partial p}{\partial x},\\
&\frac{\partial v}{\partial t}+u\frac{\partial v}{\partial x}+v\frac{\partial v}{\partial y}+fu = -\frac{1}{\rho_0}\frac{\partial p}{\partial y},\\
&0 = -\frac{\partial p}{\partial z}-\rho g,\\
&\frac{\partial u}{\partial x}+\frac{\partial v}{\partial y}+\frac{\partial w}{\partial z} = 0,\\
&\frac{\partial \rho}{\partial t}+u\frac{\partial \rho}{\partial x}+v\frac{\partial \rho}{\partial y}+w\frac{\partial \rho}{\partial z} = 0,
\end{aligned} \tag{13.125}$$

where ρ_0 is a constant reference density. We assume that the total flow is composed of a basic eastward jet $U(z)$ in geostrophic equilibrium with the basic density structure $\overline{\rho}(y,z)$ shown in Figure 13.30, plus perturbations, that is:

$$\begin{aligned}
u &= U(z)+u'(x,y,z),\\
v &= v'(x,y,z),\\
w &= w'(x,y,z),\\
\rho &= \overline{\rho}(y,z)+\rho'(x,y,z),\\
p &= \overline{p}(y,z)+p'(x,y,z).
\end{aligned} \tag{13.126}$$

The basic flow is in geostrophic and hydrostatic balance:

$$\begin{aligned} fU &= -\frac{1}{\rho_0}\frac{\partial \overline{p}}{\partial y}, \\ 0 &= -\frac{\partial \overline{p}}{\partial z} - \overline{\rho} g. \end{aligned} \tag{13.127}$$

Eliminating the pressure, we obtain the thermal wind relation:

$$\frac{dU}{dz} = \frac{g}{f\rho_0}\frac{\partial \overline{\rho}}{\partial y}, \tag{13.128}$$

which states that the eastward flow must increase with height because $\partial\overline{\rho}/\partial y > 0$. For simplicity, we assume that $\partial\overline{\rho}/\partial y$ is constant, and that $U = 0$ at the surface $z = 0$. Thus the background flow is

$$U = \frac{U_0 z}{H},$$

where U_0 is the velocity at the top of the layer at $z = H$.

We first form a vorticity equation by cross differentiating the horizontal equations of motion in (13.125), obtaining

$$\frac{\partial \zeta}{\partial t} + u\frac{\partial \zeta}{\partial x} + v\frac{\partial \zeta}{\partial y} - (\zeta + f)\frac{\partial w}{\partial z} = 0. \tag{13.129}$$

This is identical to (13.92), except for the exclusion of the β-effect here; the algebraic steps are therefore not repeated. Substituting the decomposition (13.126), and noting that $\zeta = \zeta'$ because the basic flow $U = U_0 z/H$ has no vertical component of vorticity, (13.129) becomes

$$\frac{\partial \zeta'}{\partial t} + U\frac{\partial \zeta'}{\partial x} - f\frac{\partial w'}{\partial z} = 0, \tag{13.130}$$

where the nonlinear terms have been neglected. This is the perturbation vorticity equation, which we shall now write in terms of p'.

Assume that the perturbations are large-scale and slow, so that the velocity is nearly geostrophic:

$$u' \simeq -\frac{1}{\rho_0 f}\frac{\partial p'}{\partial y}, \quad v' \simeq \frac{1}{\rho_0 f}\frac{\partial p'}{\partial x}, \tag{13.131}$$

from which the perturbation vorticity is found as

$$\zeta' = \frac{1}{\rho_0 f}\nabla_{\mathrm{H}}^2 p'. \tag{13.132}$$

We now express w' in (13.130) in terms of p'. The density equation gives

$$\frac{\partial}{\partial t}(\overline{\rho} + \rho') + (U + u')\frac{\partial}{\partial x}(\overline{\rho} + \rho') + v'\frac{\partial}{\partial y}(\overline{\rho} + \rho') + w'\frac{\partial}{\partial z}(\overline{\rho} + \rho') = 0.$$

Linearizing, we obtain

$$\frac{\partial \rho'}{\partial t} + U\frac{\partial \rho'}{\partial x} + v'\frac{\partial \overline{\rho}}{\partial y} - \frac{\rho_0 N^2 w'}{g} = 0, \tag{13.133}$$

where $N^2 = -g\rho_0^{-1}(\partial\overline{\rho}/\partial z)$. The perturbation density ρ' can be written in terms of p' by using the hydrostatic balance in (13.125), and subtracting the basic state (13.127). This gives

$$0 = -\frac{\partial p'}{\partial z} - \rho' g, \tag{13.134}$$

which states that the perturbations are hydrostatic. Equation (13.133) then gives

$$w' = -\frac{1}{\rho_0 N^2}\left[\left(\frac{\partial}{\partial t} + U\frac{\partial}{\partial x}\right)\frac{\partial p'}{\partial z} - \frac{dU}{dz}\frac{\partial p'}{\partial x}\right], \tag{13.135}$$

where we have written $\partial\overline{\rho}/\partial y$ in terms of the thermal wind dU/dz. Using (13.132) and (13.135), the perturbation vorticity equation (13.130) becomes:

$$\left(\frac{\partial}{\partial t} + U\frac{\partial}{\partial x}\right)\left[\nabla_{\mathrm{H}}^2 p' + \frac{f^2}{N^2}\frac{\partial^2 p'}{\partial z^2}\right] = 0. \tag{13.136}$$

This is the equation that governs the quasi-geostrophic perturbations on an eastward current $U(z)$.

Wave Solution

We assume that the flow is confined between two horizontal planes at $z = 0$ and $z = H$ and that it is unbounded in x and y. Real flows are likely to be bounded in the y direction, especially in a laboratory situation of flow in an annular region, where the walls set boundary conditions parallel to the flow. The boundedness in y, however, simply sets up normal modes in the form $\sin(n\pi y/L)$, where L is the width of the channel. Each of these modes can be replaced by a periodicity in y. Accordingly, we assume wavelike solutions:

$$p' = \widehat{p}\,(z)\, e^{i(kx+ly-\omega t)}. \tag{13.137}$$

The perturbation vorticity equation (13.136) then gives

$$\frac{d^2\widehat{p}}{dz^2} - \alpha^2\widehat{p} = 0, \tag{13.138}$$

where

$$\alpha^2 \equiv \frac{N^2}{f^2}(k^2 + l^2). \tag{13.139}$$

The solution of (13.138) can be written as

$$\widehat{p} = A\cosh\alpha\left(z - \frac{H}{2}\right) + B\sinh\alpha\left(z - \frac{H}{2}\right). \tag{13.140}$$

Boundary conditions have to be imposed on (13.140) in order to derive an instability criterion. These are:

$$w' = 0 \quad \text{at } z = 0, H.$$

The corresponding conditions on p' can be found from (13.135) and $U = U_0 z/H$. We obtain:

$$-\frac{\partial^2 p'}{\partial t\,\partial z} - \frac{U_0 z}{H}\frac{\partial^2 p'}{\partial x\,\partial z} + \frac{U_0}{H}\frac{\partial p'}{\partial x} = 0 \quad \text{at } z = 0, H,$$

where we have also used $U = U_0 z/H$. The two boundary conditions are therefore:

$$\frac{\partial^2 p'}{\partial t\,\partial z} - \frac{U_0}{H}\frac{\partial p'}{\partial x} = 0 \quad \text{at } z = 0,$$
$$\frac{\partial^2 p'}{\partial t\,\partial z} - \frac{U_0}{H}\frac{\partial p'}{\partial x} + U_0\frac{\partial^2 p'}{\partial x\,\partial z} = 0 \quad \text{at } z = H.$$

Instability Criterion

Using (13.137) and (13.140), the foregoing boundary conditions require:

$$A\left[\alpha c \sinh\frac{\alpha H}{2} - \frac{U_0}{H}\cosh\frac{\alpha H}{2}\right] + B\left[-\alpha c \cosh\frac{\alpha H}{2} + \frac{U_0}{H}\sinh\frac{\alpha H}{2}\right] = 0,$$
$$A\left[\alpha(U_0 - c)\sinh\frac{\alpha H}{2} - \frac{U_0}{H}\cosh\frac{\alpha H}{2}\right] + B\left[\alpha(U_0 - c)\cosh\frac{\alpha H}{2} - \frac{U_0}{H}\sinh\frac{\alpha H}{2}\right] = 0,$$

where $c = \omega/k$ is the eastward phase velocity.

This is a pair of homogeneous equations for the constants A and B. For nontrivial solutions to exist, the determinant of the coefficients must vanish. This gives, after some straightforward algebra, the phase velocity:

$$c = \frac{U_0}{2} \pm \frac{U_0}{\alpha H}\sqrt{\left(\frac{\alpha H}{2} - \tanh\frac{\alpha H}{2}\right)\left(\frac{\alpha H}{2} - \coth\frac{\alpha H}{2}\right)}. \tag{13.141}$$

Whether the solution grows with time depends on the sign of the radicand. The behavior of the functions under the radical sign is sketched in Figure 13.31. It is apparent that the first factor in the radicand is positive because $\alpha H/2 > \tanh(\alpha H/2)$ for all values of αH. However, the second factor is negative for small values of αH for which $\alpha H/2 < \coth(\alpha H/2)$. In this range the roots of c are complex conjugates, with $c = U_0/2 \pm ic_i$. Because we have assumed that the perturbations are of the form $\exp(-ikct)$, the existence of a nonzero c_i implies the possibility of a perturbation that grows as $\exp(kc_i t)$, and the solution is unstable. The marginal stability is given by the critical value of α satisfying:

$$\frac{\alpha_c H}{2} = \coth\left(\frac{\alpha_c H}{2}\right),$$

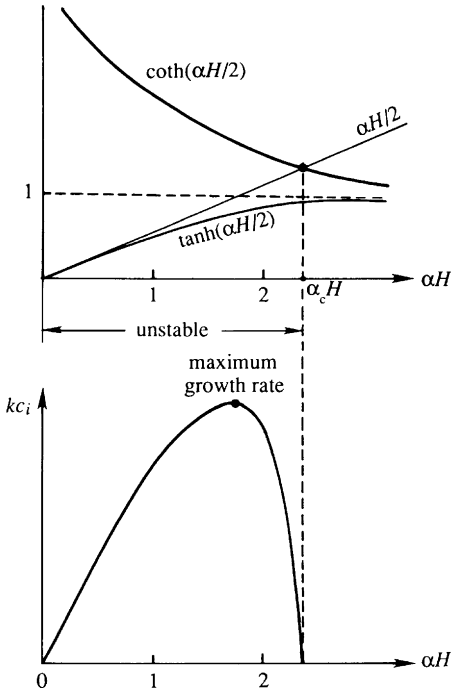

FIGURE 13.31 Baroclinic instability. The upper panel shows behavior of the functions in (13.141), and the lower panel shows growth rates of unstable waves.

whose solution is

$$\alpha_c H = 2.4,$$

and the flow is unstable if $\alpha H < 2.4$. Using the definition of α in (13.139), it follows that the flow is unstable if

$$\frac{HN}{f} < \frac{2.4}{\sqrt{k^2 + l^2}}.$$

As all values of k and l are allowed, we can always find a value of $k^2 + l^2$ low enough to satisfy the aforementioned inequality. *The flow is therefore always unstable* (*to low wave numbers*). For a north-south wave number $l = 0$, instability is ensured if the east-west wave number k is small enough such that

$$\frac{HN}{f} < \frac{2.4}{k}. \tag{13.142}$$

In a continuously stratified ocean, the speed of a long internal wave for the $n = 1$ baroclinic mode is $c = NH/\pi$, so that the corresponding internal Rossby radius is $c/f = NH/\pi f$. It is usual to omit the factor π and define the Rossby radius in a continuously stratified fluid as

$$\Lambda \equiv \frac{HN}{f}.$$

The condition (13.142) for baroclinic instability is therefore that the east-west wavelength be large enough so that

$$\lambda > 2.6\Lambda.$$

However, the wavelength $\lambda = 2.6\Lambda$ does not grow at the fastest rate. It can be shown from (13.141) that the wavelength with the largest growth rate is

$$\lambda_{\max} = 3.9\Lambda.$$

This is therefore the wavelength that is observed when the instability develops. Typical values for f, N, and H suggest that $\lambda_{\max} \sim 4000$ km in the atmosphere and 200 km in the ocean, which agree with observations. Waves much smaller than the Rossby radius do not grow, and the ones much larger than the Rossby radius grow very slowly.

Energetics

The foregoing analysis suggests that the existence of planet-encircling weather waves is due to the fact that small perturbations can grow spontaneously when superposed on an eastward current maintained by the sloping density surfaces (Figure 13.30). Although the basic current does have a vertical shear, the perturbations do not grow by extracting energy from the vertical shear field. Instead, they extract their energy from the *potential energy* stored in the system of sloping density surfaces. The energetics of the baroclinic instability is therefore quite different than that of the Kelvin-Helmholtz instability (which also has a vertical shear of the mean flow), where the perturbation Reynolds stress $\overline{u'w'}$ interacts with the vertical shear and extracts energy from the mean shear flow. The baroclinic instability is *not* a shear flow instability; the Reynolds stresses are too small because of the small w in quasi-geostrophic large-scale flows.

The energetics of the baroclinic instability can be understood by examining the equation for the perturbation kinetic energy. Such an equation can be derived by multiplying the equations for $\partial u'/\partial t$ and $\partial v'/\partial t$ by u' and v', respectively, adding the two, and integrating over the region of flow. Because of the assumed periodicity in x and y, the extent of the region of integration is chosen to be one wavelength in either direction. During this integration, the boundary conditions of zero normal flow on the walls and periodicity in x and y are used repeatedly. The procedure is similar to that for the derivation of (11.88) and is not repeated here. The result is

$$\frac{dK}{dt} = -g\int w'\rho'\,dx\,dy\,dz,$$

where K is the global perturbation kinetic energy:

$$K \equiv \frac{\rho_0}{2}\int (u'^2 + v'^2)\,dx\,dy\,dz.$$

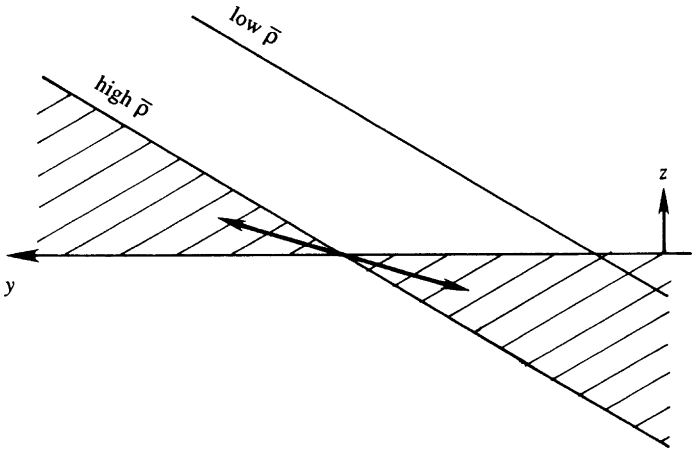

FIGURE 13.32 Wedge of instability (shaded) in a baroclinic instability. The wedge is bounded by constant density lines and the horizontal. Unstable waves have a particle trajectory that falls within the wedge and causes lighter fluid particles to move upward and northward, and heaver fluid particles to move downward and southward.

In unstable flows we must have $dK/dt > 0$, which requires that the volume integral of $w'\rho'$ must be negative. Let us denote the volume average of $w'\rho'$ by $\overline{w'\rho'}$. A negative $\overline{w'\rho'}$ means that on average the lighter fluid rises and the heavier fluid sinks. By such an interchange the center of gravity of the system, and therefore its potential energy, is lowered. The interesting point is that this cannot happen in a stably stratified system with *horizontal* density surfaces; in that case an exchange of fluid particles *raises* the potential energy. Moreover, a basic state with inclined density surfaces (Figure 13.30) cannot have $\overline{w'\rho'} < 0$ if the particle excursions are vertical. If, however, the particle excursions fall within the wedge formed by the constant density lines and the horizontal (Figure 13.32), then an exchange of fluid particles takes lighter particles upward (and northward) and denser particles downward (and southward). Such an interchange would tend to make the density surfaces more horizontal, releasing potential energy from the mean density field with a consequent growth of the perturbation energy. This type of convection is called *sloping convection*. According to Figure 13.32 the exchange of fluid particles within the *wedge of instability* results in a net poleward transport of heat from the tropics, which serves to redistribute the larger solar heat received by the tropics.

In summary, baroclinic instability draws energy from the potential energy of the mean density field. The resulting eddy motion has particle trajectories that are oriented at a small angle with the horizontal, so that the resulting heat transfer has a poleward component. The preferred scale of the disturbance is the Rossby radius.

13.18. GEOSTROPHIC TURBULENCE

Two common modes of instability of a large-scale current system were presented in the preceding sections. When the flow is strong enough, such instabilities can make a flow chaotic or turbulent. A peculiarity of large-scale turbulence in the atmosphere or the ocean is that it is essentially two dimensional in nature. The existence of the

Coriolis force, stratification, and small thickness of geophysical media severely restricts the vertical velocity in large-scale flows, which tend to be quasi-geostrophic, with the Coriolis force balancing the horizontal pressure gradient to the lowest order. Because vortex stretching, a key mechanism by which ordinary three-dimensional turbulent flows transfer energy from large to small scales, is absent in two-dimensional flow, one expects that the dynamics of geostrophic turbulence are likely to be fundamentally different from that of three-dimensional, laboratory-scale turbulence discussed in Chapter 12. However, we can still call the motion *turbulent* because it is unpredictable and diffusive.

A key result on the subject was discovered by the meteorologist Fjortoft (1953), and since then Kraichnan, Leith, Batchelor, and others have contributed to various aspects of the problem. A good discussion is given in Pedlosky (1987), to which the reader is referred for a fuller treatment. Here, we shall only point out a few important results.

An important variable in the discussion of two-dimensional turbulence is *enstrophy*, which is the mean square vorticity $\overline{\zeta^2}$. In an isotropic turbulent field we can define an energy spectrum $S(K)$, a function of the magnitude of the wave number K, as

$$\overline{u^2} = \int_0^\infty S(K)\, dK.$$

It can be shown that the enstrophy spectrum is $K^2S(K)$, that is,

$$\overline{\zeta^2} = \int_0^\infty K^2 S(K)\, dK,$$

which makes sense because vorticity involves the spatial derivatives of velocity.

We consider a freely evolving turbulent field in which the shape of the velocity spectrum changes with time. The large scales are essentially inviscid, so that both energy and enstrophy are nearly conserved:

$$\frac{d}{dt}\int_0^\infty S(K)\, dK = 0, \quad \frac{d}{dt}\int_0^\infty K^2 S(K)\, dK = 0, \tag{13.143, 13.144}$$

where terms proportional to the molecular viscosity v have been neglected on the right-hand sides of the equations. The enstrophy conservation is unique to two-dimensional turbulence because of the absence of vortex stretching.

Suppose that the energy spectrum initially contains all its energy at wave number K_0. Nonlinear interactions transfer this energy to other wave numbers, so that the sharp spectral peak smears out. For the sake of argument, suppose that all of the initial energy goes to two neighboring wave numbers K_1 and K_2, with $K_1 < K_0 < K_2$. Conservation of energy and enstrophy requires that:

$$\begin{aligned} S_0 &= S_1 + S_2, \\ K_0^2 S_0 &= K_1^2 S_1 + K_2^2 S_2, \end{aligned}$$

where S_n is the spectral energy at K_n. From this we can find the ratios of energy and enstrophy spectra before and after the transfer:

$$\frac{S_1}{S_2} = \frac{K_2 - K_0}{K_0 - K_1}\frac{K_2 + K_0}{K_1 + K_0},$$
$$\frac{K_1^2 S_1}{K_2^2 S_2} = \frac{K_1^2}{K_2^2}\frac{K_2^2 - K_0^2}{K_0^2 - K_1^2}. \tag{13.145}$$

As an example, suppose that nonlinear smearing transfers energy to wave numbers $K_1 = K_0/2$ and $K_2 = 2K_0$. Then (13.145) shows that $S_1/S_2 = 4$ and $K_1^2 S_1/K_2^2 S_2 = \frac{1}{4}$, so that more energy goes to lower wave numbers (large scales), whereas more enstrophy goes to higher wave numbers (smaller scales). This important result on two-dimensional turbulence was derived by Fjortoft (1953). Clearly, the constraint of enstrophy conservation in two-dimensional turbulence has prevented a symmetric spreading of the initial energy peak at K_0.

The unique character of two-dimensional turbulence is evident here. In three-dimensional turbulence studied in Chapter 12, the energy goes to smaller and smaller scales until it is dissipated by viscosity. In geostrophic turbulence, on the other hand, the energy goes to larger scales, where it is less susceptible to viscous dissipation. Numerical calculations are indeed in agreement with this behavior and show that energy-containing eddies grow in size by coalescing. On the other hand, the vorticity becomes increasingly confined to thin shear layers on the eddy boundaries; these shear layers contain very little energy. The backward (or inverse) energy cascade and forward enstrophy cascade are represented schematically in Figure 13.33. It is clear that there are two *inertial* regions in the spectrum of a two-dimensional turbulent flow, namely, the energy cascade region and the enstrophy cascade region. If energy is injected into the system at a rate ε, then the energy spectrum in the energy cascade region has the form $S(K) \propto \varepsilon^{2/3} K^{-5/3}$; the argument is essentially the same as in the case of the Kolmogorov spectrum in three-dimensional turbulence (Section 12.7), except that the transfer is backward. A dimensional argument also shows that the

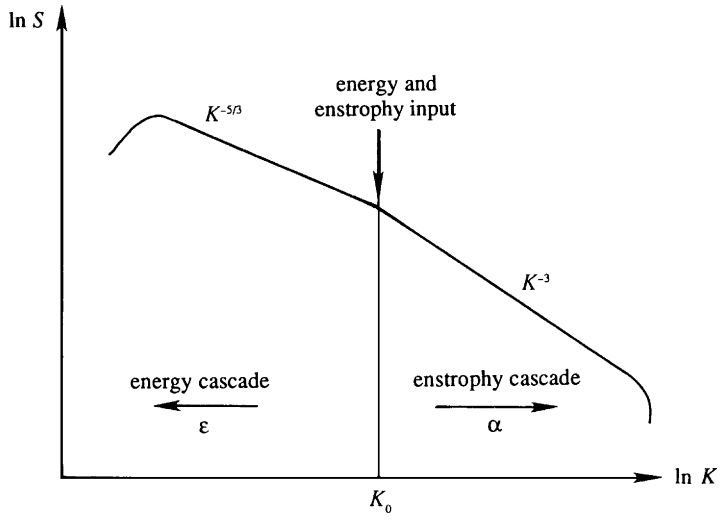

FIGURE 13.33 Energy and enstrophy cascade in two-dimensional turbulence. Here the two-dimensional character of the turbulence causes turbulent kinetic energy to cascade upward to larger scales, while enstrophy cascades to smaller scales.

energy spectrum in the enstrophy cascade region is of the form $S(K) \propto \alpha^{2/3}K^{-3}$, where α is the forward enstrophy flux to higher wave numbers. There is negligible energy flux in the enstrophy cascade region.

As the eddies grow in size, they become increasingly immune to viscous dissipation, and the inviscid assumption implied in (13.143) becomes increasingly applicable. (This would not be the case in three-dimensional turbulence in which the eddies continue to decrease in size until viscous effects drain energy out of the flow.) In contrast, the corresponding assumption in the enstrophy conservation equation (13.144) becomes less and less valid as enstrophy goes to smaller scales, where viscous dissipation drains enstrophy out of the system. At later stages in the evolution, then, (13.144) may not be a good assumption. However, it can be shown (see Pedlosky, 1987) that the dissipation of enstrophy actually *intensifies* the process of energy transfer to larger scales, so that the *red* cascade (that is, transfer to larger scales) of energy is a general result of two-dimensional turbulence.

The eddies, however, do not grow in size indefinitely. They become increasingly slower as their length scale l increases, while their velocity scale u remains constant. The slower dynamics makes them increasingly wavelike, and the eddies transform into Rossby-wave packets as their length scale becomes of order (Rhines, 1975):

$$l \sim \sqrt{\frac{u}{\beta}} \qquad \text{(Rhines length)},$$

where $\beta = df/dy$ and u is the rms fluctuating speed. The Rossby-wave propagation results in an anisotropic elongation of the eddies in the east–west ("zonal") direction, while the eddy size in the north–south direction stops growing at $\sqrt{u/\beta}$. Finally, the velocity field consists of zonally directed jets whose north–south extent is of order $\sqrt{u/\beta}$. This has been suggested as an explanation for the existence of zonal jets in the atmosphere of the planet Jupiter (Williams, 1979). The inverse energy cascade regime may not occur in the earth's atmosphere and the ocean at mid-latitudes because the Rhines length (about 1000 km in the atmosphere and 100 km in the ocean) is of the order of the internal Rossby radius, where the energy is injected by baroclinic instability. (For the inverse cascade to occur, $\sqrt{u/\beta}$ needs to be larger than the scale at which energy is injected.)

Eventually, however, the kinetic energy has to be dissipated by molecular effects at the Kolmogorov microscale η, which is of the order of a few millimeters in the ocean and the atmosphere. A fair hypothesis is that processes such as internal waves drain energy out of the mesoscale eddies, and breaking internal waves generate three-dimensional turbulence that finally cascades energy to molecular scales.

EXERCISES

13.1. The Gulf Stream flows northward along the east coast of the United States with a surface current of average magnitude 2 m/s. If the flow is assumed to be in geostrophic balance, find the average slope of the sea surface across the current at a latitude of 45°N. [*Answer*: 2.1 cm per km]

13.2. A plate containing water ($v = 10^{-6}$ m^2/s) above it rotates at a rate of 10 revolutions per minute. Find the depth of the Ekman layer, assuming that the flow is laminar.

13.3. Assume that the atmospheric Ekman layer over the earth's surface at a latitude of 45°N can be approximated by an eddy viscosity of $\nu_v = 10\ \mathrm{m}^2/\mathrm{s}$. If the geostrophic velocity above the Ekman layer is 10 m/s, what is the Ekman transport across isobars? [*Answer*: $2203\ \mathrm{m}^2/\mathrm{s}$]

13.4. Find the axis ratio of a hodograph plot for a semidiurnal tide in the middle of the ocean at a latitude of 45°N. Assume that the mid-ocean tides are rotational surface gravity waves of long wavelength and are unaffected by the proximity of coastal boundaries. If the depth of the ocean is 4 km, find the wavelength, the phase velocity, and the group velocity. Note, however, that the wavelength is comparable to the width of the ocean, so that the neglect of coastal boundaries is not very realistic.

13.5. An internal Kelvin wave on the thermocline of the ocean propagates along the west coast of Australia. The thermocline has a depth of 50 m and has a nearly discontinuous density change of $2\ \mathrm{kg/m}^3$ across it. The layer below the thermocline is deep. At a latitude of 30°S, find the direction and magnitude of the propagation speed and the decay scale perpendicular to the coast.

13.6. Using the dispersion relation $m^2 = k^2(N^2 - \omega^2)/(\omega^2 - f^2)$ for internal waves, show that the group velocity vector is given by $[c_{gx}, c_{gz}] = \dfrac{(N^2 - f^2)\,km}{(m^2 + k^2)^{3/2}(m^2 f^2 + k^2 N^2)^{1/2}}[m, -k]$. [*Hint*: Differentiate the dispersion relation partially with respect to k and m.] Show that $\mathbf{c}_g$ and $\mathbf{c}$ are perpendicular and have oppositely directed vertical components. Verify that $\mathbf{c}_g$ is parallel to $\mathbf{u}$.

13.7. Suppose the atmosphere at a latitude of 45°N is idealized by a uniformly stratified layer of height 10 km, across which the potential temperature increases by 50°C.

a) What is the value of the buoyancy frequency N?

b) Find the speed of a long gravity wave corresponding to the $n = 1$ baroclinic mode.

c) For the $n = 1$ mode, find the westward speed of nondispersive (i.e., very large wavelength) Rossby waves. [*Answer*: $N = 0.01279\ \mathrm{s}^{-1}$; $c_1 = 40.71\ \mathrm{m/s}$; $c_x = -3.12\ \mathrm{m/s}$]

13.8. Consider a steady flow rotating between plane parallel boundaries a distance L apart. The angular velocity is Ω and a small rectilinear velocity U is superposed. There is a protuberance of height $h \ll L$ in the flow. The Ekman and Rossby numbers are both small: $Ro \ll 1$, $E \ll 1$. Obtain an integral of the relevant equations of motion that relates the modified pressure and the streamfunction for the motion, and show that the modified pressure is constant on streamlines.

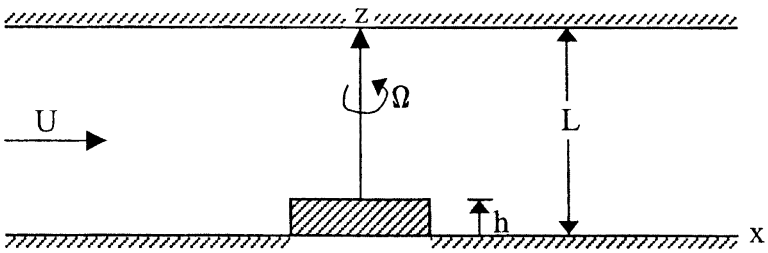

Literature Cited

Fjortoft, R. (1953). On the changes in the spectral distributions of kinetic energy for two-dimensional non-divergent flow. *Tellus, 5*, 225–230.
Gill, A. E. (1982). *Atmosphere–Ocean Dynamics*. New York: Academic Press.
Holton, J. R. (1979). *An Introduction to Dynamic Meteorology*. New York: Academic Press.
Houghton, J. T. (1986). *The Physics of the Atmosphere*. London: Cambridge University Press.
Kamenkovich, V. M. (1967). On the coefficients of eddy diffusion and eddy viscosity in large-scale oceanic and atmospheric motions. *Izvestiya, Atmospheric and Oceanic Physics, 3*, 1326–1333.
Kundu, P. K. (1977). On the importance of friction in two typical continental waters: Off Oregon and Spanish Sahara. In J. C. J. Nihoul (Ed.), *Bottom Turbulence*. Amsterdam: Elsevier.
Kuo, H. L. (1949). Dynamic instability of two-dimensional nondivergent flow in a barotropic atmosphere. *Journal of Meteorology, 6*, 105–122.
LeBlond, P. H., & Mysak, L. A. (1978). *Waves in the Ocean*. Amsterdam: Elsevier.
McCreary, J. P. (1985). Modeling equatorial ocean circulation. *Annual Review of Fluid Mechanics, 17*, 359–409.
Munk, W. (1981). Internal waves and small-scale processes. In B. A. Warren, & C. Wunch (Eds.), *Evolution of Physical Oceanography*. Cambridge, MA: MIT Press.
Pedlosky, J. (1971). Geophysical fluid dynamics. In W. H. Reid (Ed.), *Mathematical Problems in the Geophysical Sciences*. Providence, Rhode Island: American Mathematical Society.
Pedlosky, J. (1987). *Geophysical Fluid Dynamics*. New York: Springer-Verlag.
Phillips, O. M. (1977). *The Dynamics of the Upper Ocean*. London: Cambridge University Press.
Prandtl, L. (1952). *Essentials of Fluid Dynamics*. New York: Hafner Publ. Co.
Rhines, P. B. (1975). Waves and turbulence on a β-plane. *Journal of Fluid Mechanics, 69*, 417–443.
Stommel, H. (1948). The westward intensification of wind-driven ocean currents. *Transactions, American Geophysical Union, 29*(2), 202–206.
Taylor, G. I. (1915). Eddy motion in the atmosphere. *Philosophical Transactions of the Royal Society of London, A215*, 1–26.
Williams, G. P. (1979). Planetary circulations: 2. The Jovian quasi-geostrophic regime. *Journal of Atmospheric Sciences, 36*, 932–968.

Supplemental Reading

Chan, J. C. L. (2005). The physics of tropical cyclone motion. *Annual Review of Fluid Mechanics, 37*, 99–128.
Haynes, P. (2005). Stratospheric dynamics. *Annual Review of Fluid Mechanics, 37*, 263–293.
Wiggins, S. (2005). The dynamical systems approach to Lagrangian transport in oceanic flows. *Annual Review of Fluid Mechanics, 37*, 295–328.